https://doi.org/10.5194/egusphere-2026-4210
Preprint. Discussion started: 22 July 2026

Improving Shortwave Radiative Transfer in the Lake Component of the Common Land Model (CoLM-Lake) with a Spectral Scheme for the Full Snow-Ice-Water Column

Xueqi Cao[1], Nan Wei[1*], Hua Yuan[1], Shupeng Zhang[1], Zhongwang Wei[1], Xingjie Lu[1], Lu Li[1], and Yongjiu Dai[1]

[1]School of Atmospheric Sciences, Sun Yat-sen University, Zhuhai 519082, China

Correspondence to: Nan Wei (wein6@mail.sysu.edu.cn)

Abstract. Shortwave radiation controls lake thermal structure and ice evolution, yet one-dimensional lake models typically use bulk Beer–Lambert attenuation in water and optically opaque snow and ice. Here, treating the full snow-ice-water column as a unified, optically active system, we couple the Snow, Ice, and Aerosol Radiation Model with Adding-Doubling version 5 (SNICAR-ADv5) with the lake component of the Common Land Model (CoLM-Lake) to represent spectral radiative transfer for lake columns. The coupled model accounts for wavelength-dependent absorption and scattering, direct and diffuse pathways, Fresnel interface effects, and radiative interactions among layers. We evaluate the coupled model across nine lakes spanning depth, clarity, climate, and ice cover. Its impacts are physically consistent but lake dependent. During open-water periods, the coupled model shifts absorbed shortwave energy toward near-surface, especially for diffuse radiation, and reduces heating below the mixed layer. This behavior improves temperature profiles and thermocline depths where the original model overheats below the mixed layer and places thermoclines too deep. In turbid lakes, observation-based water extinction coefficients provide first-order improvements, whereas the spectral scheme gives a more interpretable heating profile than single-band Beer–Lambert attenuation. During ice-covered periods, it partitions shortwave energy among snow, ice, and water, enabling representation of internal ice heating, under-ice warming, and basal melt. Limited improvements in some deep or clear lakes indicate that radiative transfer advances must be combined with improved mixing and heat storage. This implementation provides a process-based tool for diagnosing and improving lake thermal, ice, and lake–atmosphere interaction simulations in land, weather, and Earth system models.

1 Introduction

Lakes exert critical effects on the Earth system. They modulate land surface energy and water balances, alter planetary boundary-layer and convection-trigger conditions, and thereby influence atmospheric temperature, moisture, and precipitation

https://doi.org/10.5194/egusphere-2026-4210
Preprint. Discussion started: 22 July 2026

patterns from local to regional scales (Kirillin et al., 2021; Ma et al., 2024; Notaro et al., 2013; Scott and Huff, 1996; Verpoorter et al., 2014; Yao et al., 2023). As a result, numerical weather, climate and Earth system models commonly include lake models to represent lake–atmosphere interactions, aiming to improve the fidelity of extreme-event forecasts and climate change projections (Bernus and Ottlé, 2022; Gu et al., 2015; Ma et al., 2022; Subin et al., 2012). Over the past decades, lake models have developed along two complementary tracks: three-dimensional (3-D) hydrodynamic models which resolve lake horizontal structures and transfer processes of mass, momentum and energy; and vertically resolved one-dimensional (1-D) models which idealize lakes as horizontally homogeneous columns (Cole and Wells, 2006; Dai et al., 2018; Luijendijk, 2001; MacKay et al., 2009; Mironov et al., 2010; Stepanenko et al., 2016; Tan et al., 2015). While 3-D models provide more mechanistic details, especially for large or morphologically complex lakes, 1-D models are more widely used in regional and global simulations due to their simplified parameterization schemes, high computational efficiency, and suitability for small lakes which constitute the vast majority of global lake systems and can be reasonably approximated as horizontally homogeneous (M. Guo et al., 2021; MacKay et al., 2009; Mironov et al., 2010; Subin et al., 2012). Therefore, enhancing the performance of 1-D lake models remains of great value for land-atmosphere interaction studies and weather and climate model developments.

Previous studies have shown that physical parameterization schemes of 1-D lake models contain multiple sources of uncertainty which can induce significant biases and inter-model differences in simulated lake thermal regimes. These include the parameterizations of surface momentum, sensible and latent heat fluxes, the representation of shortwave radiation absorption at the lake surface and with depth, the treatment of turbulent mixing processes within water bodies, particularly for those driven by wind under stable stratification, and the formulation of water-sediment heat transport and exchange (Desgué-Itier et al., 2023; M. Guo et al., 2021; Ma et al., 2022; Stepanenko et al., 2013, 2014; Su et al., 2019; Q. Zhang et al., 2019). Among these uncertainties, the representation of shortwave radiation absorption and attenuation within water bodies as well as overlying snow and ice layers when they exist serves as the dominant contributor. Solar radiation is the major energy input controlling the overall lake energy budget and heat deposition (Tong et al., 2023; W. Wang et al., 2018; Xu et al., 2016). Its vertical penetration within the entire lake system directly determines the vertical heating profile and thus the lake thermal structure. Consequently, oversimplified shortwave radiation transfer schemes and inaccurate specification of water optical properties can significantly impair the ability of lake models to simulate mixed-layer evolution, stratification strength, the timing and magnitude of overturning events, and evaporation efficiency (A. Huang et al., 2019; L. Huang et al., 2021; Kirillin et al., 2017; Lazhu et al., 2021; M. Wang et al., 2022; Xiao et al., 2020; Zhou et al., 2023). Shortwave radiation transfer schemes can be even more unreliable during ice-covered periods. Properties of snow and ice such as spatiotemporally varied albedo and spectral extinction coefficients, which are difficult to measure or simulate precisely, strongly modulate the partitioning of incident radiation among snow, ice and water layers, and hence biases in radiative transfer through snow and ice substantially affect simulated snow cover freeze-thaw cycles, lake ice phenology, and under-ice water overturn (Dang et al., 2016; Riihelä et al., 2021; Wang et al., 2022; R. Zhang et al., 2019; Zhou et al., 2023). Given the central role of radiative

https://doi.org/10.5194/egusphere-2026-4210
Preprint. Discussion started: 22 July 2026

heating in both open-water and ice-covered conditions, traditional shortwave radiation transfer schemes used in 1-D lake models warrant systematic reevaluation to identify avenues for further development.

1-D lake models typically adopt simplified radiative-transfer treatments: (1) under open-water conditions, incoming shortwave radiation is partitioned at the surface and attenuated with depth following the Beer-Lambert law with empirical extinction coefficients; (2) under ice-covered conditions, sunlight is assumed to be absorbed by the top snow or ice layer (Dai et al., 2018; A. Huang et al., 2019; Z. Li et al., 2021; Subin et al., 2012). These treatments are conceptually straightforward and computationally efficient, but they rely on strong assumptions such as spectrally uniform absorption, negligible scattering, low-transparency snow and ice, and time- and depth-invariant optical properties, which are frequently violated in real lakes. Some models introduce a small set of band-averaged extinction coefficients or lake-specific snow-ice-water extinction profiles obtained by parameter calibration, which indeed better reproduce observed phenomena such as under-ice warming and accelerated ice melt (W. Huang et al., 2022; Kirillin et al., 2021; Z. Li et al., 2021; M. Wang et al., 2022; Zolfaghari et al., 2017). However, fundamental structural deficiencies in radiative-transfer representation persist, and thus systematic biases in lake thermal structures remain unsolved. Therefore, 1-D lake models would benefit from upgrades toward physically based radiative-transfer schemes, such as multi-band two-stream approximations, explicit treatment of scattering, or coupling to radiative transfer models that account for effects of lake water quality and biogeochemistry, to address the aforementioned limitations.

A typical class of radiative transfer models is based on solving the one-dimensional radiative transfer equation for plane-parallel, vertically inhomogeneous media. For example, the Discrete Ordinates Radiative Transfer (DISORT) solver computes the scalar radiative transfer equation in vertically inhomogeneous, plane-parallel media while accounting for absorption, multiple scattering, and thermal release. The discrete-ordinates method replaces the angular scattering integral with a numerical quadrature over a finite set of propagation directions, namely streams, yielding a system of coupled ordinary differential equations in optical depth (Stamnes et al., 1988). Increasing the number of streams generally improves the representation of angular radiance distributions, particularly in strongly anisotropic scattering conditions, but also substantially increases the computational cost. Consequently, although DISORT is widely used for detailed radiative-transfer calculations and benchmark studies, operational weather and climate models generally employ more computationally efficient or reduced-order schemes. By contrast, the two-stream approximation reduces the angularly resolved radiation field to upward and downward hemispheric fluxes. It can approximately account for absorption, reflection, and multiple scattering while substantially reducing computational cost relative to multi-stream methods (Briegleb, 1992). The two-stream approximation therefore provides a practical compromise between physical fidelity and computational efficiency. It has been widely adopted in the radiative transfer schemes of general circulation models. For example, the Rapid Radiative Transfer Model for GCMs (RRTMG) combines efficient two-stream calculations with spectral parameterizations to calculate atmospheric radiative fluxes and heating rates (Iacono et al., 2008). Two-stream approximation is also commonly used in vegetation radiative transfer schemes, where the canopy is generally represented as a horizontally homogeneous turbid medium and the upward and downward radiation fluxes are calculated from canopy optical properties (Dai et al., 2004). These applications demonstrate the

https://doi.org/10.5194/egusphere-2026-4210
Preprint. Discussion started: 22 July 2026

computational efficiency and flexibility of the two-stream approximation across different layered media. Therefore, the two-stream approximation represents a promising approach for describing shortwave radiative transfer in 1-D lake models, provided that water-column optical properties and air–water and water–sediment boundary conditions are appropriately represented.

The Snow, Ice, and Aerosol Radiation model (SNICAR), which is developed to simulate spectral radiative transfer within layered media using the two-stream approximation method, can be a promising candidate for improving radiative treatments in 1-D lake models. Early implementations of SNICAR emphasized accurate calculation of spectral albedo and solar-energy absorption in layered snow, and a stable version (Adv3) has therefore been incorporated into multiple land surface models such as the Community Land Model (CLM), the Common Land Model (CoLM), the Energy Exascale Earth System Land Model (ELM), and the Noah with multi-parameterization options (Noah-MP) to improve snow albedo representation (S. Guo et al., 2025; Hao et al., 2023; C. He et al., 2024; Lin et al., 2025). Recent releases of SNICAR have extended its applicability to ice and water surfaces (Flanner et al., 2021; Tolento et al., 2024; Whicker et al., 2022). The latest version ADv5 further accounts for Fresnel reflection at the air–water interface under the assumption that the interface is horizontally flat. These extensions provide the potential of SNICAR to improve the simulation of lake thermal dynamics, through a consistent treatment of snow–ice–water as a single optically unified system. They can effectively and efficiently capture spectral dependence, anisotropic scattering, and inter-medium radiative transfer in a lake system, and thus coupling SNICAR with 1-D lake models is expected to substantially enhance the physical realism of simulated radiative heating profiles and, consequently, lake thermal structures.

To improve the representation of shortwave radiative transfer in 1-D lake models, this study employs the SNICAR-ADv5 radiative-transfer scheme to replace the original CoLM-Lake (the lake module used in CoLM) exponential-attenuation scheme. The upgraded scheme explicitly represents direct and diffuse fluxes, resolves spectral dependence and scattering, and treats inter-media transmission by accounting for Fresnel reflection at interfaces among snow, ice, and water. We evaluate the coupled model across nine lakes chosen to span a wide range of optical properties, depths, and climatic forcings, comparing the new scheme with the original single-band exponential formulation and with available observations. The study has two principal objectives: (1) to advance the physical fidelity of shortwave radiative-transfer parameterizations in 1-D lake models; (2) to quantify the applicability and limitations of the spectral two-stream approximation relative to the traditional single-band exponential attenuation (Beer-Lambert law) for simulating lake thermal state, mixed-layer evolution, ice phenology, and lake–atmosphere interactions.

2 Methods

2.1 Brief description of the original shortwave radiative treatment in CoLM-Lake

CoLM-Lake is a 1-D turbulence-diffusion lake model derived from the framework of Hostetler and Bartlein (1990). It represents the snow-ice-water-sediment column as a vertically resolved system and simulates time-evolving vertical profiles

https://doi.org/10.5194/egusphere-2026-4210
Preprint. Discussion started: 22 July 2026

of temperature and ice fraction by accounting for heat conduction, phase changes, and vertical mixing. The surface energy balance (including net shortwave and longwave radiation, and sensible and latent heat fluxes) is solved iteratively for the lake-air interface temperature. Heat transfer between raindrops and the lake surface is also included to represent precipitation effects on the upper-layer thermodynamic state. Within the water column, vertical heat transport is represented by an eddy-diffusivity formulation that combines molecular diffusion, a wind-driven large-eddy term, and an empirically diagnosed enhanced diffusivity to account for unresolved processes. Stability-based convective mixing is applied to maintain monotonic density profiles. Detailed descriptions and evaluations of CoLM-Lake are provided by Dai et al. (2018) and Huang et al. (2019).

CoLM-Lake treats shortwave radiative transfer according to the lake surface state. Under frozen conditions, snow albedo is calculated as in CoLM for non-lake subgrids (Flanner and Zender, 2006), and lake ice albedo is prescribed as 0.6 in the visible band and 0.4 in the near-infrared band (Subin et al., 2012). After the reflected component is removed from the total incident shortwave radiation, all remaining solar energy is assumed to be absorbed by the top snow or ice layer, as snow and ice are treated as effectively opaque. Under unfrozen conditions, the albedo for direct shortwave radiation is calculated as $\alpha = 0.05/(\cos Z + 0.15)$, where Z is the solar zenith angle, and the diffuse albedo is prescribed as 0.1 (Subin et al., 2012). For the net solar radiation entering the lake column, a fraction β (typically set as the near-infrared portion) is assumed to be absorbed at the surface, and a prescribed absorption depth z_a defines the water depth directly affected by this surface absorption. The remaining solar radiation is distributed into subsurface layers below z_a using an extinction coefficient η, so that the residual downwelling solar flux at depth z is given by:

$$\phi(z) = (1-\beta)S_g \exp[-\eta(z - z_a)] \quad (1)$$

where S_g (W m^{-2}) denotes the net solar flux available to the lake column. CoLM-Lake sets z_a as a simple function of lake depth d:

$$z_a = \begin{cases} 0.5 \text{ m}, & d < 4 \text{ m} \\ 0.6 \text{ m}, & d \geq 4 \text{ m} \end{cases} \quad (2)$$

and adopts an empirical depth-dependent expression for η for practical use:

$$\eta = 1.1925 d^{-0.424} \quad (3)$$

These implementations make the shortwave radiative transfer scheme computationally cheap and robust for long integrations, but they inherit typical structural limitations: (1) single-band treatment, which artificially confines near-infrared radiation to a prescribed surface layer and attenuates the remaining visible-band radiation via a single exponential decay, both imposed as fixed parameterizations rather than determined by spectral optical properties; (2) neglect of scattering, which omits the oblique and upward photon paths that increase effective optical path length, particularly for diffuse radiation, and biases absorption along depth; (3) opaque snow/ice assumptions, which prevent the model from representing internal ice heating, under-ice warming, and basal melt; and (4) empirically prescribed albedo decoupled from subsurface optical physics, which suppresses snow/ice-albedo feedbacks and makes the surface energy partition insensitive to changes in snow grain size, ice bubble content, impurity loading, and water quality. These deficiencies suggest that the original scheme can systematically misrepresent both

https://doi.org/10.5194/egusphere-2026-4210
Preprint. Discussion started: 22 July 2026

the surface partition of radiation among reflection and transmission into subsurface, and the vertical distribution of absorbed solar energy among subsurface layers. They motivate a physically based replacement in which spectral resolution, scattering, interfacial transmission, and unified optical calculations are consistently represented.

2.2 Updates of shortwave radiative transfer representation in CoLM-Lake induced by SNICAR-ADv5

To overcome the above limitations, we couple the Snow, Ice, and Aerosol Radiation Model with Adding-Doubling version 5 (SNICAR-ADv5) with CoLM-Lake, replacing the original shortwave radiative treatment and embedding it as a two-way coupled component within the CoLM-Lake timestep loop. The coupled model improves the representation of shortwave radiative transfer in four key aspects: spectrally resolved radiative transfer, explicit treatment of scattering, multi-layer radiative coupling across optically active snow, ice, and water layers, and a unified Fresnel interface treatment that allows surface albedo to emerge physically from the optical properties of the layered medium (Tolento et al., 2024). These four aspects are described in detail in the following subsections. The thermodynamic and mixing calculations retain the original formulations in CoLM-Lake (Dai et al., 2018; Huang et al., 2019), while the radiative heating calculated by the coupled scheme is passed into these existing routines to produce the updated lake thermal structure at each timestep.

2.2.1 Spectrally resolved shortwave radiative transfer

The first structural limitation of the original scheme is its single-band Beer-Lambert attenuation, which assumes that the near-infrared fraction is arbitrarily absorbed within a fixed surface layer and the remainder follows a single exponential extinction profile. This treatment does not reflect the actual spectral dependence of solar energy absorption. In the coupled scheme, the shortwave radiative transfer is resolved in the five spectral broadbands used by CoLM-Lake (0.3–0.7, 0.7–1.0, 1.0–1.2, 1.2–1.5, and 1.5–5.0 μm). The penetration depth of each band is determined by its wavelength-specific absorption and scattering coefficients. The near-infrared radiation, with extinction coefficients that are orders of magnitude larger than those in the visible band, attenuates naturally within the uppermost millimeters to centimeters of the water column, whereas visible-band radiation propagates substantially deeper. The vertical heating profile thus emerges directly from the spectral optical calculations rather than being prescribed through an empirical parameterization. For a monochromatic beam, the radiative transfer equation is expressed as:

$$\mu\frac{dI}{d\tau}+I=\frac{\omega}{4\pi}\int_{4\pi}P(\Omega,\Omega')I(\Omega',\tau)d\Omega' \quad (4)$$

where μ is the cosine of the solar zenith angle, τ is the extinction optical depth, I is the radiance (W m^{-2} sr^{-1}), ω is the single-scattering albedo, P is the scattering phase function (sr^{-1}), and Ω denotes the solid angle (sr). In the numerical implementation, the incident shortwave flux is separated into direct-beam and diffuse components before it enters the layered column. The direct beam is solved for a specified incident zenith angle and is attenuated along the corresponding slant optical path, and scattering transfers part of the direct radiation into diffuse radiation represented by upward and downward fluxes. The diffuse

https://doi.org/10.5194/egusphere-2026-4210
Preprint. Discussion started: 22 July 2026

component is treated as an angularly integrated ensemble of direct-beam solutions evaluated over the downward hemisphere using Gaussian quadrature angles. This treatment retains the different geometrical effects of direct and diffuse illumination, which are lost when all transmitted radiation is assigned a single vertical Beer-Lambert attenuation profile. Thus, the coupled scheme solves the radiative transfer equation with explicit separation of direct and diffuse illumination, zenith-angle-dependent slant-path attenuation, and scattering-mediated coupling between the two radiation streams.

2.2.2 Explicit treatment of scattering via the two-stream approximation

The second structural limitation of the original scheme is the neglect of scattering. The scattering-free Beer-Lambert formulation omits oblique and upward photon pathways that can increase effective optical path length, particularly for diffuse radiation, and therefore biases absorption along depth. In the coupled scheme, scattering is represented using the two-stream approximation, in which the angular radiation field is reduced to two hemispherically integrated fluxes: a downward-propagating flux and an upward-propagating flux that are coupled through scattering processes. This formulation does not explicitly solve the full scattering phase function in Equation 4. Instead, it parameterizes the phase function through the asymmetry factor g, defined as the mean cosine of the scattering angle. Values of g close to 1 indicate that scattering is strongly concentrated in the forward direction, $g = 0$ corresponds to isotropic scattering, and negative g indicates predominantly backward scattering.

In the lake column, the asymmetry factor differs substantially among the three constituent media. For snow grains, whose effective radii are typically large relative to solar wavelengths (Mie-scattering regime), scattering is strongly forward-peaked, with g typically in the range of 0.85–0.97. Lake ice shows similarly high g values because scattering by air bubbles and ice grains also falls in the Mie regime, though the exact value depends on bubble size and ice density. For liquid water, in contrast, scattering by water molecules is in the Rayleigh regime, producing nearly symmetric forward–backward scattering with $g = 0$. These contrasting asymmetry factors pose a challenge for the two-stream framework: in snow and ice, the narrowly forward-peaked phase function cannot be adequately resolved when only two hemispheric directions are retained, yet the forward scattering has a first-order effect on the vertical penetration of radiation. To address this challenge, the coupled scheme employs the delta-Eddington approximation (Joseph et al., 1976), in which the strong forward peak of the scattering phase function is removed and the optical properties are rescaled using the forward-scattering fraction f ($f = g^2$):

$$\tau^* = (1 - \omega f)\tau, \quad \omega^* = \frac{(1 - f)\omega}{1 - \omega f}, \quad g^* = \frac{g - f}{1 - f} \tag{5}$$

The delta-Eddington scaling preserves the leading effect of forward scattering on radiative fluxes while reducing the angular complexity of the transfer problem, which makes the scheme computationally suitable for lake model integrations.

https://doi.org/10.5194/egusphere-2026-4210
Preprint. Discussion started: 22 July 2026

2.2.3 Optically active snow, ice, and water media with multi-layer adding-doubling solver for shortwave radiative transfer

The third structural limitation of the original scheme is the assumption that snow and ice are optically opaque. This assumption prevents the model from representing internal snow/ice heating, under-ice radiative warming, and basal melt, all of which are critical processes for realistic lake simulation (Huang et al., 2022; Kirillin et al., 2021). The coupled scheme removes this opaque-layer assumption by treating snow, ice, and water as optically active media, with absorption, scattering, and transmission explicitly resolved within each layer. In contrast to the original scheme, which confines all shortwave absorption to the top frozen layer, the coupled scheme allows radiation to propagate through snow and ice and enter the underlying water. The transmitted flux is governed by layer-specific optical properties. A thick snowpack, with its high scattering and extinction coefficients, strongly attenuates incident radiation, such that most shortwave energy is absorbed or scattered within the upper snow layers and only a small residual flux reaches the ice or water beneath. Lake ice, by contrast, generally exhibits weaker scattering and greater optical transparency. Thin, bubble-poor ice can transmit a substantial fraction of incident radiation to the sub-ice water, whereas thick, bubble-rich ice enhances scattering, reduces transmission, and increases internal absorption. Radiation that reaches the water column can drive under-ice warming and, when sufficient energy is available, contribute to basal melt. These transmission pathways are absent in the original scheme.

To solve the radiative transfer equations across this multi-layer snow–ice–water column, the coupled scheme uses the adding–doubling (AD) algorithm (Briegleb, 1992; Briegleb and Light, 2007). Rather than solving the equations with one global tridiagonal matrix system, the AD approach first derives the apparent optical response of each individual layer, including its diffuse reflectance and transmittance, and then combines adjacent layers recursively. During this layer-adding procedure, radiation can be repeatedly reflected and transmitted across layer boundaries. Thus, the resulting reflectance and transmittance represent the cumulative effect of multiple internal radiative interactions within the full snow-ice-water column. In addition, for the lake application, a key advantage of the AD framework is that it naturally accommodates internal Fresnel interfaces. The original tridiagonal-matrix solver used in earlier versions of SNICAR places the Fresnel treatment only at the upper boundary (Toon et al., 1989), whereas the AD solver allows reflective and refractive interfaces to be inserted between any pair of layers, which makes it possible to treat snow, ice, and water as a unified optical column with physically consistent interfacial reflection and transmission at all internal boundaries. The AD solver also offers other benefits over the tridiagonal formulation, including higher accuracy for albedo under diffuse illumination, better numerical stability across a wide range of solar zenith angles, and lower computational cost. The advantages of the AD solver in SNICAR are summarized by Dang et al. (2019).

2.2.4 Unified Fresnel interface treatments

The fourth structural limitation of the original CoLM-Lake radiative treatment is that surface albedo is prescribed as fixed constants or diagnosed from an empirical formula, which is decoupled with the optical properties that govern subsurface absorption. The coupled scheme removes this inconsistency by calculating Fresnel reflection and refraction at interfaces between optically distinct media using Snell's law and the Fresnel equations. This treatment is applied at all possible boundaries

https://doi.org/10.5194/egusphere-2026-4210
Preprint. Discussion started: 22 July 2026

in a lake system: air–snow, snow–ice, air–ice, ice–water, and air–water boundaries. Therefore, surface albedo and interfacial transmission emerge from the same spectral optical calculation used for within-layer absorption and scattering, rather than being imposed independently as prescribed boundary parameters. The coupled framework enables CoLM-Lake to treat snow cover, lake ice, and underlying water as a unified optical column and to simulate the vertical redistribution of solar energy more physically.

Figure 1 illustrates the main radiative pathways represented in the coupled CoLM-Lake and SNICAR-ADv5 framework. Incoming solar radiation propagates downward through the snow, ice, and water layers, where it undergoes scattering and absorption within each medium and transmission across all existing interfaces represented by Fresnel reflection and refraction. Part of the radiation is ultimately reflected back to the atmosphere after interacting with the lake system, while the remainder is progressively attenuated and absorbed within the lake column and underlying sediment.

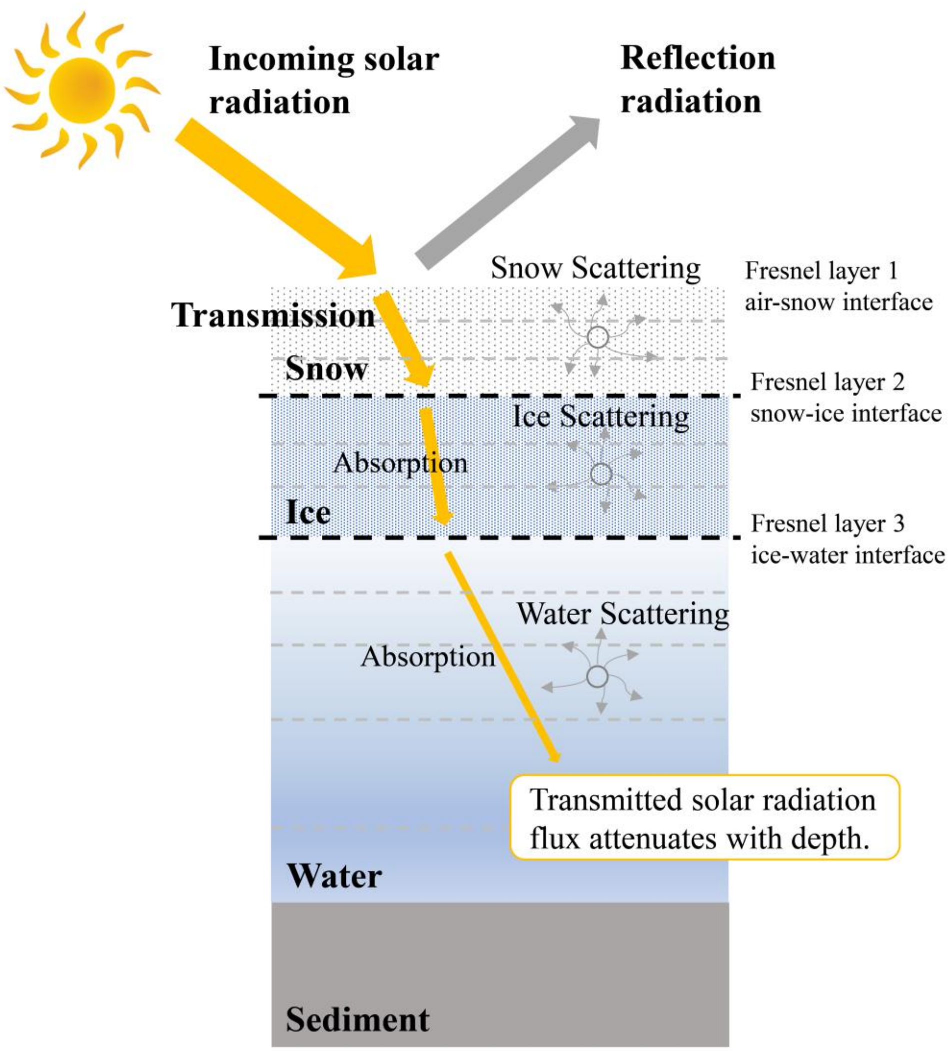

https://doi.org/10.5194/egusphere-2026-4210
Preprint. Discussion started: 22 July 2026

Figure 1. Schematic representation of shortwave radiative transfer in the coupled CoLM-Lake and SNICAR-ADv5 framework. The coupled scheme represents spectral absorption, scattering, transmission, and Fresnel reflection/refraction across the snow-ice-water column.

2.3 Parameter settings in SNICAR-ADv5 coupled with CoLM-Lake

SNICAR-ADv5 requires three fundamental inherent optical properties for all constituent media to represent shortwave radiative transfer: the single-scattering albedo, extinction coefficient, and asymmetry parameter. These properties are largely obtained from the SNICAR-ADv5 optical property database, which provides band-specific values over the full 0.3-5.0 μm spectral range divided into 480 narrow bands (Tolento et al., 2024). These values are derived from Mie-scattering theory, and thus can provide a physically based description of wavelength-dependent absorption and scattering in a lake column. Because CoLM-Lake employs five broadband shortwave intervals rather than the 480-band spectral discretization, all optical properties are aggregated into the CoLM-Lake spectral framework using band-weighted averaging. For each broadband interval, the weight assigned to a narrow band is its fractional contribution to the incoming spectral energy under a specified atmospheric spectral distribution. SNICAR-ADv5 provides multiple spectral distributions of solar radiation under different atmospheric conditions, and the midlatitude winter atmospheric profile is selected in this study. This aggregation ensures consistency between the detailed SNICAR-ADv5 optical database and the computationally efficient broadband formulation implemented in CoLM-Lake. The specific parameter configurations of optical properties for snow, ice, liquid water, and Fresnel interfaces are described below.

2.3.1 Parameter settings of snow

For snowpack, the optical properties required by SNICAR-ADv5 are specified for both snow grains and eight species of light-absorbing aerosols deposited within snow. The five-band single-scattering albedo, extinction coefficient, and asymmetry parameter for the light-absorbing aerosols are obtained by spectrally averaging the corresponding values from the SNICAR optical-property database over the broadband intervals used in CoLM-Lake, which are listed in Tables S1-S3. The corresponding optical properties for snow grains are also taken from the SNICAR optical-property database, but they depend on snow effective radius. During the simulation, the snow effective radius is updated dynamically as the snow ages through dry metamorphism, wet metamorphism, refreezing, and new-snow deposition (Brun, 1989; Flanner and Zender, 2006). The layer-mean effective radius is then calculated as a mass-weighted combination of the contributions from pre-existing snow, newly fallen snow, and refrozen ice. Snow grain shape also affects the asymmetry parameter, but it is assumed to be spherical in this study, and thus this effect is neglected to simplify the scattering calculations.

2.3.2 Parameter settings of ice

For lake ice, the optical properties required by SNICAR-ADv5 are specified for ice grains and black carbon across the same five broadband intervals used in CoLM-Lake. The optical properties of black carbon in ice are assumed to be identical to those

https://doi.org/10.5194/egusphere-2026-4210
Preprint. Discussion started: 22 July 2026

used for black carbon in snow. For ice grains, the scattering coefficient, asymmetry parameter, and complex refractive index are obtained from the SNICAR optical-property database, and the database provides the scattering coefficient and asymmetry parameter as a function of the air-bubble radius within ice. The absorption coefficient is computed from the imaginary part of the complex refractive index as $k_{\mathrm{abs}} = 4\pi \mathrm{Im}(m_{ice})/\lambda$, where $\mathrm{Im}(m_{ice})$ denotes the imaginary component of the complex refractive index and λ is the wavelength of each broadband. The single-scattering albedo and extinction coefficients of ice are subsequently calculated from the scattering and absorption coefficients, and the bulk optical thickness of lake ice is then computed from the extinction coefficients, effective ice density, and equivalent black carbon concentration.

The aforementioned three required microphysical parameters of lake ice, namely the air-bubble radius, effective ice density, and equivalent black carbon concentration, are difficult to obtain because observations are limited, but they strongly affect the detailed behavior of shortwave radiative transfer within ice. The air-bubble radius and effective ice density jointly determine scattering by altering ice-air interfaces. At a fixed ice density, larger bubbles generally imply a lower bubble number and a smaller specific surface area, which weakens volume scattering, lowers albedo, and allows more shortwave radiation to penetrate downward. Conversely, lower-density ice contains a larger air-volume fraction and more ice-air interfaces, which strengthens scattering, increases albedo, and reduces transmittance. Equivalent black-carbon concentration primarily controls visible-band absorption. A higher impurity loading can darken the ice, enhance internal radiative heating, and reduce the radiation transmitted to the underlying water. To obtain more reliable optical properties for lake ice, a parameter-inversion procedure using the offline SNICAR-ADv5 model is applied to retrieve these unknown ice microphysical parameters that can most closely reproduce bare-ice albedo observed by the Moderate Resolution Imaging Spectroradiometer (MODIS). This procedure largely follows the inversion workflow of Whicker et al. (2024). For lakes with sufficient observational coverage, snow-free ice periods are first isolated so that the inversion would not be contaminated by overlying snow. Bare-ice scenes are identified from the MODIS reflectance (MOD09GA) and snow (MOD10A1) products by requiring MOD09GA Band 2 reflectance > 0.11, Band 4 reflectance > 0.10, and Band 2 reflectance < 0.60 (Hall et al., 2002; Shimada et al., 2016), together with MOD10A1 Normalized Difference Snow Index (NDSI) snow cover < 100 to retain observations with cloud-free conditions. For these periods, the quality-screened albedo from Band 2 (a near-infrared band) of the MCD43A3 product is used as the primary target to identify the combination of effective ice density and air-bubble radius that minimizes the mismatch between modeled and observed albedo. The MCD43A3 product in Band 2 is strongly sensitive to ice microstructures but relatively insensitive to atmospheric light-absorbing impurities (Schneider et al., 2019), and thus it can reduce the influence of atmospheric contamination on retrieved ice microstructural parameters. The candidate ranges of the ice microstructural parameters are constrained using in situ measurements, with effective ice density restricted to 900-917 kg m^{-3} and air-bubble radius to 100-1500 μm (Chang et al., 2023; Chevrollier et al., 2023; Cuffey and Paterson, 2010; Dadic et al., 2013). After the ice microstructural properties are determined, the inversion is repeated using the visible-band albedo from the MCD43A3 product to estimate the equivalent black carbon concentration. This step exploits the stronger sensitivity of the visible spectrum to ice impurity loading and surface darkening, allowing the parameter to be adjusted until the simulated albedo best matches

https://doi.org/10.5194/egusphere-2026-4210
Preprint. Discussion started: 22 July 2026

the MODIS observations. Together, these inversion steps yield a self-consistent set of lake-ice microphysical parameters and optical properties, which are used for the subsequent coupled SNICAR-ADv5 and CoLM-Lake simulations.

2.3.3 Parameter settings of water

For lake water, the optical properties required by SNICAR-ADv5 are specified for liquid water only. The five-band scattering coefficient, complex refractive index, and asymmetry parameter of liquid water are taken from the SNICAR optical-property database. The absorption coefficient is computed using the same formulation as for ice but with the refractive index of liquid water. The extinction coefficient is then obtained as the sum of the scattering and absorption coefficients, and the single-scattering albedo is calculated as the ratio of the scattering coefficient to the extinction coefficient. In addition, because observed extinction coefficients in the visible band are available from the Inter-Sectoral Impact Model Intercomparison Project 2a (ISIMIP2a) or from site-specific literature (Table 1), the visible-band extinction coefficient is set using those observed values. This treatment preserves the physically based spectral optical properties while incorporating site-level constraints, and it also partially accounts for the optical influences of lake-water quality or suspended sediments since the observed extinction coefficient reflects the integrated optical property of lake water.

2.3.4 Parameter settings at Fresnel interfaces

At Fresnel interfaces, radiative reflection and refraction are calculated using Snell's law and the Fresnel equations. The interfacial optical property is expressed using the relative refractive index, defined as the ratio of the complex refractive index of the lower medium to that of the upper medium along the photon propagation path (Briegleb and Light, 2007). This treatment allows SNICAR-ADv5 to represent interfacial transmission and reflection consistently across the full snow-ice-water column in CoLM-Lake. The complex refractive indices of air and snow for the interfacial Fresnel calculations are assumed to be 1, whereas those of lake ice and liquid water are taken from the SNICAR optical-property database which is based on the Picard et al. (2016) parameterization and Segelstein (1981) dataset.

2.4 Experimental design

Three numerical experiments are conducted for each selected lake to quantify the effects of successive improvements to the shortwave radiative treatment in CoLM-Lake on simulated lake thermal evolution:

1. CoLM-Default: This experiment uses the standard CoLM-Lake configuration with its original parameterizations. In this baseline setup, shortwave radiative transfer through snow and ice is not explicitly resolved, and the lake water extinction coefficient is estimated using the default empirical depth-dependent formulation.

2. CoLM-Extinct: This experiment retains all default physics of CoLM-Lake except that the empirical lake water extinction formulation is replaced by the observation-based value. This experiment isolates the effect of correcting only the bulk optical attenuation of lake water on simulated lake thermal structure.

https://doi.org/10.5194/egusphere-2026-4210
Preprint. Discussion started: 22 July 2026

3. CoLM-Snicar: This experiment further replaces the default scheme of shortwave radiative transfer in CoLM-Lake with SNICAR-ADv5 while retaining the observation-based visible-band water extinction coefficient. In contrast to CoLM-Default and CoLM-Extinct where all near-infrared solar radiation is absorbed at the surface while visible radiation penetrates the lake water following a simplified attenuation formulation, CoLM-Snicar explicitly simulates shortwave radiation transfer across five spectral broadbands. It represents scattering, reflection, transmission, and absorption throughout the full snow-ice-water column, together with the optical effects of aerosol impurities and snow and ice microstructure.

These three experiments provide a stepwise framework for evaluating the added value of improved shortwave radiative parameterization in CoLM-Lake.

In all experiments, the lake depth at each site is set as the average of the deepest measurement depth of the validation data and the reported maximum lake depth compiled from the literature or data sources listed in Table 1. Meteorological forcing is provided by site-specific automatic observing stations for all lakes except Lake Nam Co, where the atmospheric forcing is taken from the China Meteorological Forcing Data version 2 (CMFDv2) (J. He et al., 2025). All simulations use the same source of monthly global wet and dry deposition fluxes of black carbon, dust, and organic carbon, which are taken from the Community Earth System Model-Whole Atmosphere Community Climate Model (CESM2-WACCM) simulations participating in Coupled Model Intercomparison Project Phase 6 (CMIP6) (Danabasoglu et al., 2020). In all experiments, the lake depth at each site is set as the average of the deepest measurement depth of the validation data and the reported maximum lake depth compiled from the literature or data sources listed in Table 1. Meteorological forcing is provided by site-specific automatic observing stations for all lakes except Lake Nam Co, where the atmospheric forcing is taken from the China Meteorological Forcing Data version 2 (CMFDv2) (J. He et al., 2025). All simulations use the same source of monthly global wet and dry deposition fluxes of black carbon, dust, and organic carbon, which are taken from the Community Earth System Model-Whole Atmosphere Community Climate Model (CESM2-WACCM) simulations participating in Coupled Model Intercomparison Project Phase 6 (CMIP6) (Danabasoglu et al., 2020).

2.5 Evaluation metrics

Model performance is evaluated using five standard statistical metrics: the root mean square error (RMSE), the relative root mean square error (RRMSE), bias, relative bias, and the Pearson correlation coefficient.

RMSE measures the absolute magnitude of the difference between simulated and observed values, whereas RRMSE normalizes this error by the mean of the observations to provide a scale-independent measure of model performance. These two metrics are used together to assess both lake-specific simulation errors and relative model skill across lakes with different thermal regimes and morphometric characteristics.

Bias quantifies the mean directional deviation of the simulations from the observations, with positive values indicating overestimation and negative values indicating underestimation. Relative bias expresses this deviation as a percentage of the observed mean, allowing proportional errors to be compared across lakes, depths, and variables. The Pearson correlation

https://doi.org/10.5194/egusphere-2026-4210
Preprint. Discussion started: 22 July 2026

coefficient is used to evaluate the linear temporal agreement between simulations and observations. Higher correlation values indicate that the model better captures the timing of seasonal lake thermal evolution, including convective overturn, stratification onset and decay, and mixed-layer development.

The evaluation is conducted using daily mean model outputs and observations. Depending on data availability at each site, the statistical analysis is performed over different temporal windows, ranging from full annual cycles to shorter seasonal periods. To ensure a direct comparison between simulations and measurements, the simulated lake temperature profiles are vertically interpolated to the corresponding observational depths before the metrics are calculated.

3 Data

3.1 In-situ observations

In this study, nine lake sites are selected to evaluate the performance of CoLM-Lake coupled with SNICAR-ADv5 under different morphometric and optical conditions. These sites are broadly classified into shallow lakes, medium-depth lakes, and one deep lake as listed in Table 1. They span a wide range of water clarity, with light extinction coefficients varying from 0.08 to 7.08 m^{-1}, allowing the model to be tested across radiative environments from highly transparent to strongly turbid lakes. Model evaluation focuses on the evolution of lake water temperature profiles at all nine sites, and on lake ice phenology at sites with available observations of ice freeze-up and break-up dates. Validation data are obtained from site-specific measurements. For lakes without explicitly reported lake water extinction coefficients, values are taken from the ISIMIP2a database (Marcé et al., 2022); for lakes with only Secchi Disk Depth available, extinction coefficients are estimated using the empirical relationship established by Zhang et al. (2020). For most lakes whose simulation periods include ice-covered conditions, lake-ice microphysical parameters are derived using the parameter-inversion procedure described in Section 2.3.2. The inversion is not performed for Lake Harp and Ngoring because reliable observations for snow-free bare ice albedo cannot be obtained from MODIS. The ice surface of Lake Harp is snow-covered for most of the observation period and therefore does not satisfy the snow-free bare ice screening criteria. For Lake Ngoring, frequent cloud cover degrades the quality of MODIS albedo retrievals and prevents the observations from meeting the inversion quality requirements. For these two lakes, the default lake ice microphysical parameters provided by SNICAR-ADv5 are used. Together, these nine site datasets provide the in situ constraints needed to assess model performances across diverse thermal, optical, and ice-covered regimes.

Table 1. Basic information and simulation setup for the selected lakes in this study

	Lake name	**Location**	**Lake water extinction[1] (m^{-1})**	**Lake depth (m)**	**Meteorological forcing sources**	**Variables to be evaluated**	**Lake ice microphysical parameters**	**Simulation periods**	**Data references**

https://doi.org/10.5194/egusphere-2026-4210
Preprint. Discussion started: 22 July 2026

Shallow lakes	Crystal Bog	46.01° N, 89.61° W	0.963	2.38	Local automatic observing station	Lake water temperature, Lake ice phenology	Parameter inversion	2016/11-2018/03	Magnuson et al. (2023a)
	Kossenblatter	52.13° N, 14.1°E	7.08	2	Local automatic observing station	Lake water temperature	-	2003/05-2003/11	Beyrich et al. (2006)
	Tai	31.4°N, 120.22° E	3.62	2	Local automatic observing station	Lake water temperature	-	2010/06-2011/06	Lee et al. (2014)
Medium-depth lakes	Harp	45.58° N, 79.13° W	0.36	32.3	Local automatic observing station	Lake water temperature	Default values in SNICAR[2]	2010/07-2015/10	Yao et al. (2014)
	Trout	46.03° N, 89.67° W	0.314	32.85	Local automatic observing station	Lake water temperature, Lake ice phenology	Parameter inversion	2016/11-2018/03	Magnuson et al. (2026a)
	Sparkling	46.01° N, 89.7°W	0.239	18	Local automatic observing station	Lake water temperature	Parameter inversion	2019/03-2020/03	Magnuson et al. (2026b)
	Trout Bog	46.04° N, 89.69° W	1.3	7.83	Local automatic observing station	Lake water temperature, Lake ice	Parameter inversion	2016/11-2018/03	Magnuson et al. (2023b)

						phenology			
	Ngoring	34.9°N, 97.7°E	0.3	30.34	Local automatic observing station	Lake water temperature, Lake ice phenology	Default values in SNICAR	2015/11-2016/06	Kirillin et al. (2021)
Deep Lake	Nam Co	30.76°N, 90.78°E	0.08	92	China Meteorological Forcing Data (version 2)	Lake water temperature	Parameter inversion	2012/01-2013/12	Lazhu et al. (2016)

[1] Lake water extinction coefficients are taken from Subin et al. (2012) for Lake Kossenblatter and from Wu et al. (2024) for Lake Nam Co; that for Lake Tai is estimated from Secchi disk depth using an empirical relationship (Zhang et al., 2020); and the others are obtained from the ISIMIP2a database (Marcé et al., 2022).

[2] The parameter inversion for lake ice microphysical properties is not performed for Lake Harp and Ngoring because reliable observations for snow-free bare ice albedo cannot be obtained from MODIS. The default parameter values provided by SNICAR-ADv5 (0.75 mm for air-bubble radius, 910 kg m^{-3} for effective ice density, and 0 for equivalent black carbon concentration) are used.

3.2 MODIS derived products

This study uses three MODIS Collection products at 500 m resolution: MOD09GA surface reflectance, MOD10A1 snow cover, and MCD43A3 albedo. These datasets are combined to identify snow-free lake-ice periods and to derive quality-controlled lake-ice albedo observations. Lake-ice surfaces are first screened using MOD09GA Band 2 and Band 4 reflectance to distinguish frozen lake surfaces from snow and open water. Cloud-contaminated periods are further removed using the MOD10A1 NDSI snow cover product. Based on the selected lake-ice periods, only MCD43A3 retrievals with BRDF_Albedo_Band_Mandatory_Quality = 0 are retained for the corresponding spectral bands to ensure the data quality of lake ice albedo. The resulting dataset provides spatially and temporally consistent MODIS-based lake-ice albedo observations for parameter inversion of lake ice microphysics.

3.3 Other auxiliary datasets

Ice thickness data are required as inputs for the offline SNICAR-ADv5 model in the parameter-inversion procedure. The hemispheric-scale lake ice thickness dataset of Li et al. (2022) provides model-derived ice thickness for Lake Nam Co. In-situ ice thickness observations from Magnuson et al. (2023c)are also used to obtain ice thickness data for the selected North

https://doi.org/10.5194/egusphere-2026-4210
Preprint. Discussion started: 22 July 2026

American lakes, including Lake Trout, Sparkling, Trout Bog, and Crystal Bog. These datasets provide the ice geometry needed to constrain the inversion of lake ice parameters.

4 Results

4.1 Model performances for shallow lakes

Lake Crystal Bog is selected as the representative shallow lake for diagnosing the differences among the three experiments because it is seasonally ice covered, and develops a pronounced summer thermal gradient. The observations show a rapid transition after ice-off from an almost vertically homogeneous spring water column to a strongly stratified summer state. During peak stratification, the warmest water is confined mainly to the upper 0.5-1.0 m where temperature approaches nearly 25 °C, whereas the bottom water remains below approximately 16 °C (Fig. 2a). Thus, Lake Crystal Bog provides a stringent test of whether CoLM-Lake can represent both the seasonal evolution and the vertical distribution of heat in shallow lakes.

The default model is unable to reproduce the observed vertical thermal structure of Lake Crystal Bog. In CoLM-Default, temperature variations are dominated by seasonal changes rather than by depth (Fig. 2b), indicating simulated excessive vertical mixing. The resulting bias is small near the surface but becomes strongly positive at depth, with the bottom water several degrees warmer than observed throughout most of the open-water season (Fig. 2e). Replacing the default empirical extinction coefficient with the observation-based value in CoLM-Extinct produces only negligible changes relative to CoLM-Default (Fig. 2c and 2f). This weak response is reasonable for Lake Crystal Bog because the observed extinction coefficient (0.963 m^{-1}) is close to the depth-dependent default value used by CoLM-Default (0.826 m^{-1}). Therefore, for this lake, only correcting the extinction coefficient cannot suppress the overestimated vertical mixing, and the simplified single-band exponential attenuation treatment for radiation transfer could be the principal deficiency for the simulated biases.

As expected, CoLM-Snicar substantially alters the simulated thermal regime of Lake Crystal Bog. The model captures the development of a warm epilimnion, a sharp thermocline, and a cooler hypolimnion during summer (Fig. 2d). Relative to CoLM-Extinct, CoLM-Snicar produces only modest changes in the uppermost layer but cools the water below about 1 m by approximately 2-4 °C during the stratified season (Fig. 2g). This cooling strongly reduces the warm bias in the lower part of the water column and brings the simulated vertical profiles much closer to the observations.

https://doi.org/10.5194/egusphere-2026-4210
Preprint. Discussion started: 22 July 2026

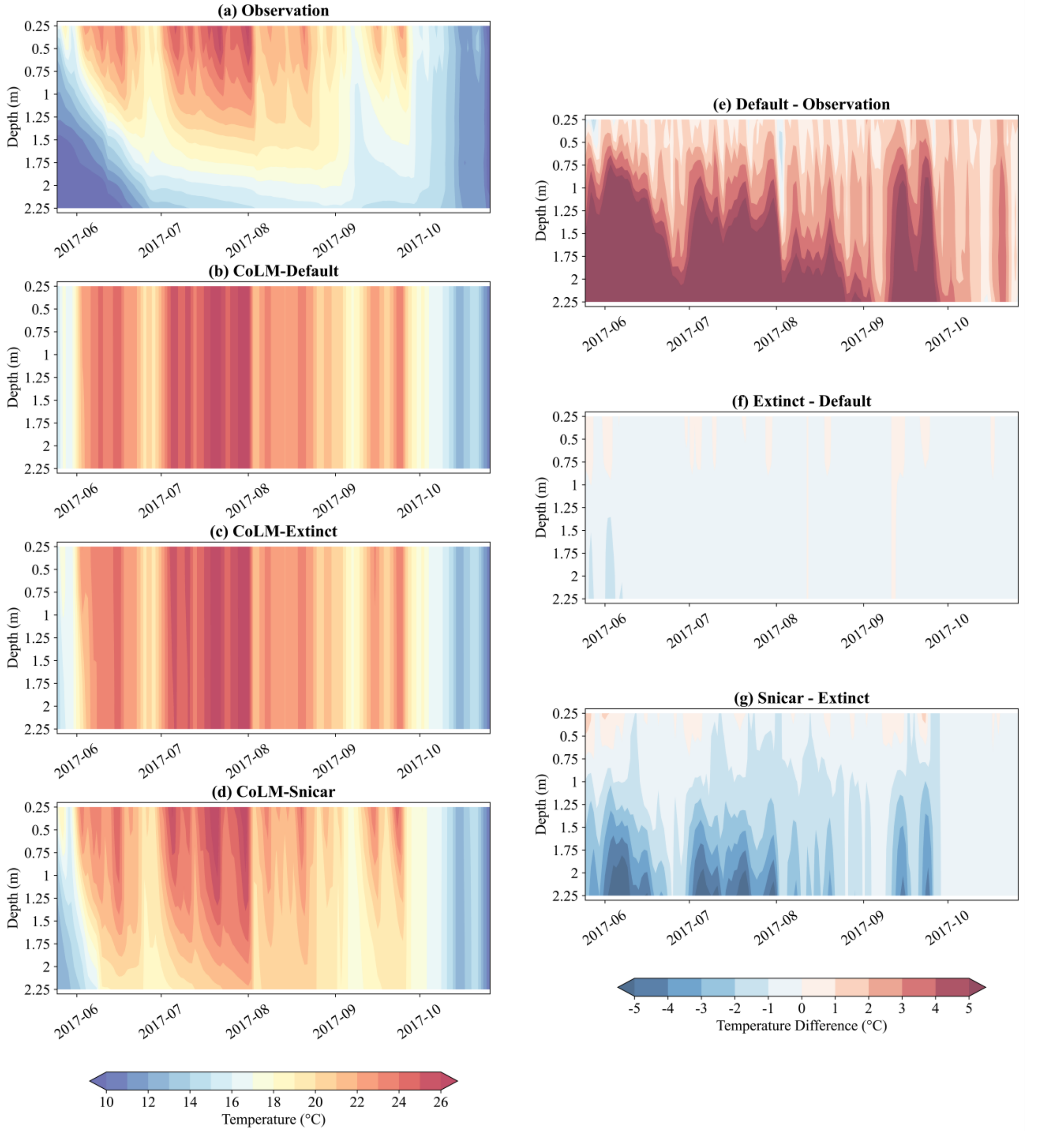

Figure 2. Observed and simulated daily-mean water-temperature profiles in Lake Crystal Bog. (a) Observations; (b-d) simulations from CoLM-Default, CoLM-Extinct, and CoLM-Snicar, respectively; (e-g) simulated differences between CoLM-Default and observations, CoLM-Extinct and CoLM-Default, and CoLM-Snicar and CoLM-Extinct, respectively.

https://doi.org/10.5194/egusphere-2026-4210
Preprint. Discussion started: 22 July 2026

The depth-dependent statistical evaluation further supports the benefit of SNICAR-ADv5 in simulated lake water temperature profiles of Lake Crystal Bog. In the upper 1 m, all three experiments capture the seasonal temperature evolution reasonably well, with the values of temporal correlation (TC) generally above 0.9 and RMSE values of about 1-2 °C (Fig. 3a and 3c). Below this depth, however, the performances of CoLM-Default and CoLM-Extinct deteriorate rapidly. Their warm biases and RMSEs increase almost monotonically with depth, reaching about 7-8 °C near the lake bottom, while TC decreases to below 0.4 (Fig. 3). The nearly overlapping blue and green curves confirm again that using the observed extinction coefficient alone does not correct the excessively warm and weakly stratified deep-water state. CoLM-Snicar reduces these depth-dependent errors in a systematic way. At deep measurement levels, the warm bias and RMSE are reduced by about 3-4 °C compared with CoLM-Default and CoLM-Extinct, and TC remains above approximately 0.6 rather than collapsing below 0.4 (Fig. 3). These results demonstrate that introducing SNICAR-ADv5 in CoLM-Lake improves not only the mean vertical thermal structure but also the timing of subsurface warming and cooling. The improvement is most pronounced in the lower water column, suggesting that the default radiative-transfer treatment deposits too much heat in deeper layers.

https://doi.org/10.5194/egusphere-2026-4210
Preprint. Discussion started: 22 July 2026

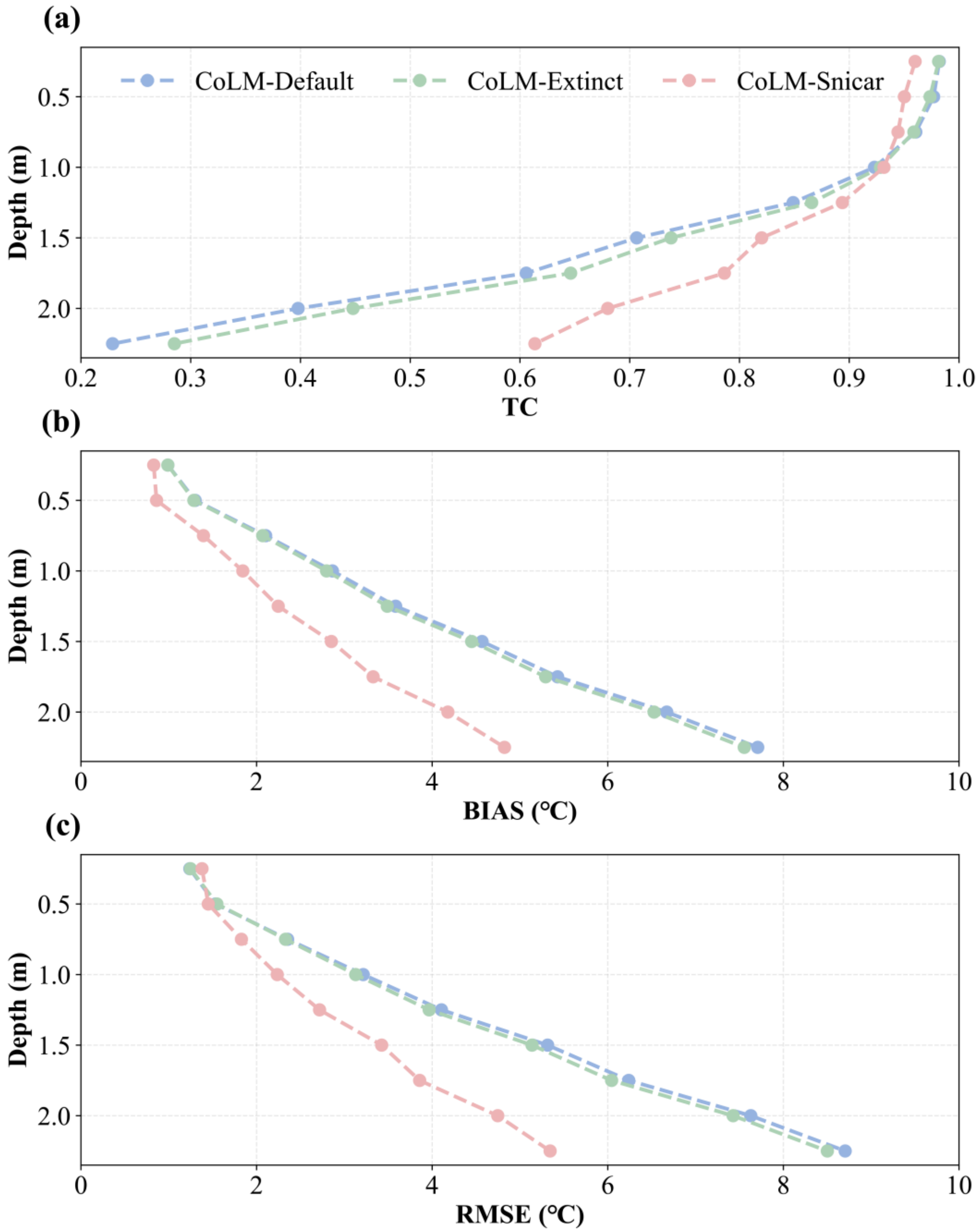

Figure 3. Depth-resolved performance statistics for simulated daily-mean water temperature in Lake Crystal Bog. (a) Pearson temporal correlation (TC); (b) bias, calculated as simulation minus observation; and (c) root mean square error (RMSE). The three curves compare CoLM-Default, CoLM-Extinct, and CoLM-Snicar against observations.

To identify the direct reason for the improved simulated deep-layer temperatures of Lake Crystal Bog, we examine the layer-by-layer absorption of direct and diffuse shortwave radiation in CoLM-Extinct and CoLM-Snicar (Fig. 4). During the open-

https://doi.org/10.5194/egusphere-2026-4210
Preprint. Discussion started: 22 July 2026

water season, the dominant signal in CoLM-Snicar is an upward redistribution of absorbed solar energy relative to CoLM-Extinct. In the upper 0-0.5 m layers, CoLM-Snicar increases the absorption of both direct and diffuse radiation, with the diffuse component showing a larger increase, up to about 10 W m^{-2} (Fig. 4e and 4f). This enhanced near-surface absorption is accompanied by reduced absorption below 0.5 m, where the energy deficit reaches roughly 2-10 W m^{-2}, especially for diffuse radiation. The redistribution of absorbed solar energy directly explains the stronger stratification and smaller hypolimnetic warm bias in CoLM-Snicar. The shift of the absorbed solar energy toward the near-surface, especially for the diffuse component, is probably due to the explicitly resolved spectral scattering processes in SNICAR-ADv5, which limits heat input into the deeper water layers. This mechanism will be further elaborated in the discussion section. In addition, we also check the column-integrated absorbed shortwave radiation during the open-water season (Fig. S1). The total absorbed direct radiation differs little between CoLM-Snicar and CoLM-Extinct, whereas total absorbed diffuse radiation is consistently larger in CoLM-Snicar, commonly by about 2-7 W m^{-2}. Thus, the simulated cooler deep water in CoLM-Snicar occurs despite an increase in total solar radiation absorption. This apparent contrast further underscores that the key role of SNICAR-ADv5 in Lake Crystal Bog is to redistribute the vertical absorption of solar energy within the water column.

During the frozen season of Lake Crystal Bog, the differences between CoLM-Extinct and CoLM-Snicar depend on whether snow overlies the lake ice. When snow is present, CoLM-Snicar permits a fraction of incident shortwave radiation to enter the upper snowpack, but the large snow scattering and extinction coefficients attenuate this radiation rapidly. Consequently, little residual energy reaches the underlying ice or water (Fig. 4b and 4d). During ice-covered but snow-free periods, the lower scattering and higher transparency of lake ice allow shortwave radiation to penetrate through the ice and heat the sub-ice water. Under this condition, CoLM-Snicar produces an additional nearly 4 W m^{-2} of absorbed energy in the upper water layers relative to CoLM-Extinct (Fig. 4e and 4f). These processes are absent in CoLM-Default and CoLM-Extinct because both experiments treat snow and ice as optically opaque, with all incoming radiation absorbed in the uppermost snow or ice layer.

https://doi.org/10.5194/egusphere-2026-4210
Preprint. Discussion started: 22 July 2026

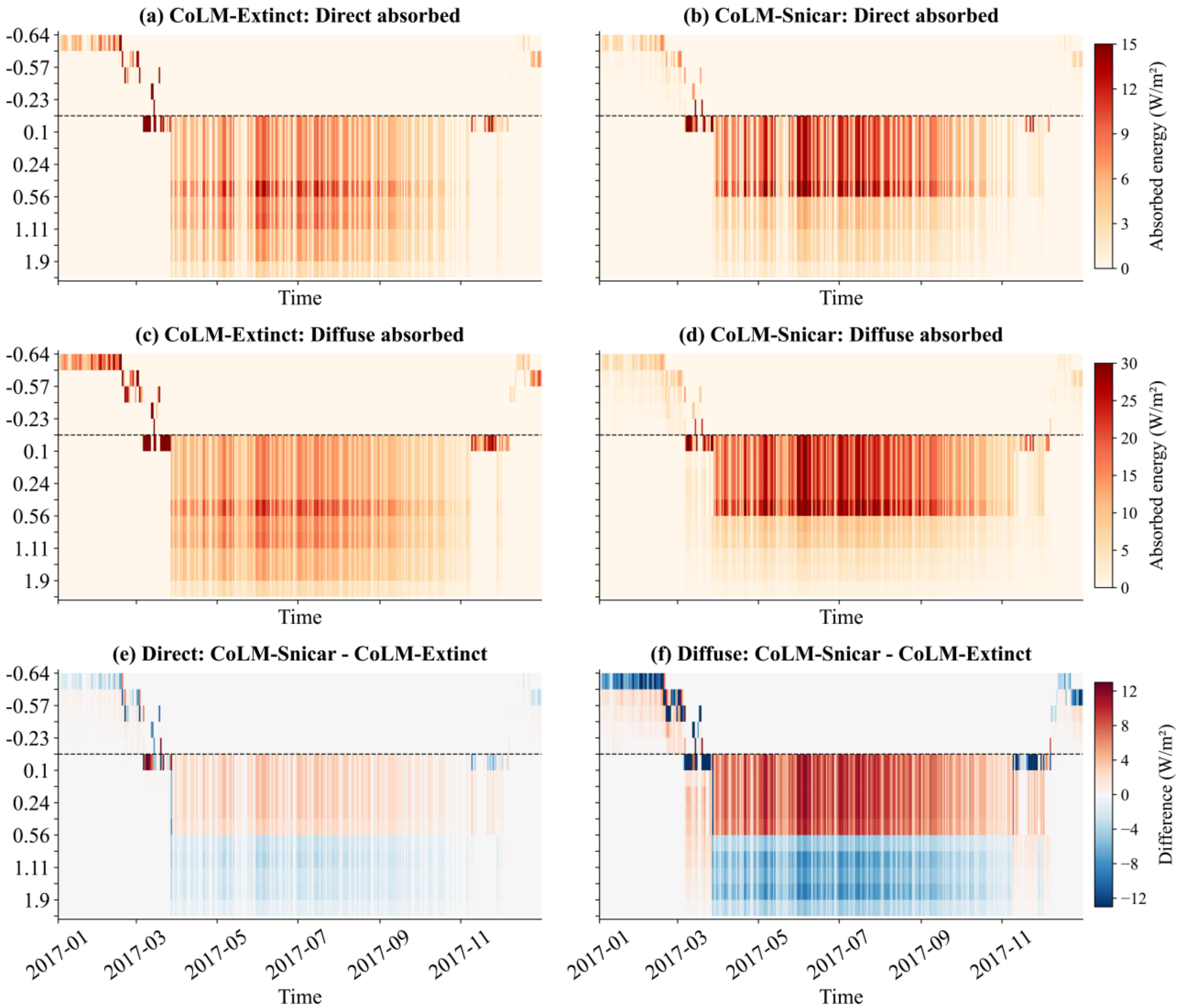

Figure 4. Layer-by-layer absorbed shortwave radiation in Lake Crystal Bog during 2017. (a-b) Direct-radiation absorption in CoLM-Extinct and CoLM-Snicar; (c-d) diffuse-radiation absorption in CoLM-Extinct and CoLM-Snicar; and (e-f) differences in absorbed direct and diffuse radiation between CoLM-Snicar and CoLM-Extinct. The dashed black line separates the snowpack from the underlying ice and water layers. Positive values in (e-f) indicate larger absorption in CoLM-Snicar. In CoLM-Extinct, solar radiation is absorbed only by the uppermost snow layer when snow is present, or by the uppermost ice layer during snow-free ice-covered periods.

Overall, Figs. 2-4 indicate that the advantage of CoLM-Snicar for Lake Crystal Bog arises from a physically more realistic partitioning of shortwave energy among snow, ice, and water, and from a shallower deposition of energy during the open-water season. The resulting increase in near-surface heating and decrease in deep-water heating maintain a stronger epilimnion-

https://doi.org/10.5194/egusphere-2026-4210
Preprint. Discussion started: 22 July 2026

hypolimnion contrast and suppress the excessive vertical mixing produced by the default radiative-transfer scheme in CoLM-Lake.

The same qualitative response of CoLM-Lake to coupling SNICAR-ADv5 can be found in the other two shallow lakes, Lake Tai and Kossenblatter (Figs. S2 and S3). In both cases, CoLM-Snicar simulates lower temperatures in the deeper layers than CoLM-Default during open-water seasons, indicating reduced unrealistic penetration of solar heat into the lower water column. However, unlike Lake Crystal Bog, these two lakes are highly turbid and have observed extinction coefficients (3.62 m^{-1} for Lake Tai and 7.08 m^{-1} for Lake Kossenblatter) that are much larger than the default depth-based estimates. As a result, CoLM-Extinct alone provides a substantial improvement by increasing upper-layer solar heat trapping and cooling the lower water column. In Lake Tai, the use of the observed extinction coefficient clearly improves the simulated water temperatures at 1.0-1.5 m (Fig. S2), indicating that the bulk extinction coefficient is a first-order control. In Lake Kossenblatter, both CoLM-Extinct and CoLM-Snicar greatly reduce lower-layer warming relative to CoLM-Default (Fig. S3). These cases show that, for shallow turbid lakes, an accurate extinction coefficient is essential, while SNICAR-ADv5 further provides a physically consistent representation of spectral absorption, scattering, and interfacial transmission. Across all shallow lake cases, the common effect of SNICAR-ADv5 is to restrict unrealistically deep solar heat penetration and to favor the development of stronger thermal stratification.

4.2 Model performances for moderately deep lakes

Lake Harp is selected as the representative medium-depth lake because it combines seasonal snow and ice cover with a well-developed open-water stratification. This lake is sufficiently deep to maintain a relatively stable hypolimnion, but its mixed layer and metalimnion still respond strongly to seasonal radiative heating. It therefore can be used to test whether CoLM-Lake coupled with the new snow-ice-water radiative-transfer treatment can improve the simulated mixed-layer evolution and thermocline position without degrading the deep-water thermal state.

The observations show that Lake Harp develops a clear summer thermocline, with the warmest water confined mainly to the upper few meters and a mixed-layer thickness of approximately 4-6 m during the stratified season (Fig. 5a). CoLM-Default captures the seasonal onset and decay of stratification, but it simulates the thermal transition too deep in the water column (Fig. 5b). This produces a typical biased thermal pattern: the uppermost layers remain too cold during summer, whereas excessive heat is transported into the metalimnion and upper hypolimnion, where warm biases exceed 2 °C and locally become much larger (Fig. 5e). Thus, the main deficiency of CoLM-Lake for Lake Harp can be characterized as an overly deep mixed layer and an overly broad thermocline, which leads to the simulated thermal biases.

Replacing the empirical water extinction formulation with the site-specific extinction coefficient in CoLM-Extinct moderately improves the simulated vertical structure (Fig. 5c). Relative to CoLM-Default, CoLM-Extinct warms the near-surface layers by about 0.5-1.0 °C and cools the middle and deeper layers by about 1-2 °C during the open-water season (Fig. 5f). These changes sharpen the vertical temperature gradient and reduce part of the warm bias below the observed thermocline.

https://doi.org/10.5194/egusphere-2026-4210
Preprint. Discussion started: 22 July 2026

Nevertheless, the simulated mixed layer remains too deep, indicating that the use of a better bulk extinction coefficient alone cannot fully correct the simulated vertical thermal pattern.

CoLM-Snicar provides the largest improvement among the three experiments (Fig. 5d). Compared with CoLM-Extinct, it further warms the upper 2-3 m by approximately 0.5-1.2 °C while cooling the water beneath the thermocline by about 0.5-3.0 °C during the summer (Fig. 5g). This additional adjustment produces a thinner and more realistic mixed layer and shifts the simulated thermocline closer to the observed depth. The added value of SNICAR-ADv5 in Lake Harp is therefore expressed mainly as an improvement in simulated mixed-layer thickness, thermocline depth, and metalimnion temperature, rather than as the creation of stratification from a fully mixed state as observed in the cases of shallow lakes.

https://doi.org/10.5194/egusphere-2026-4210
Preprint. Discussion started: 22 July 2026

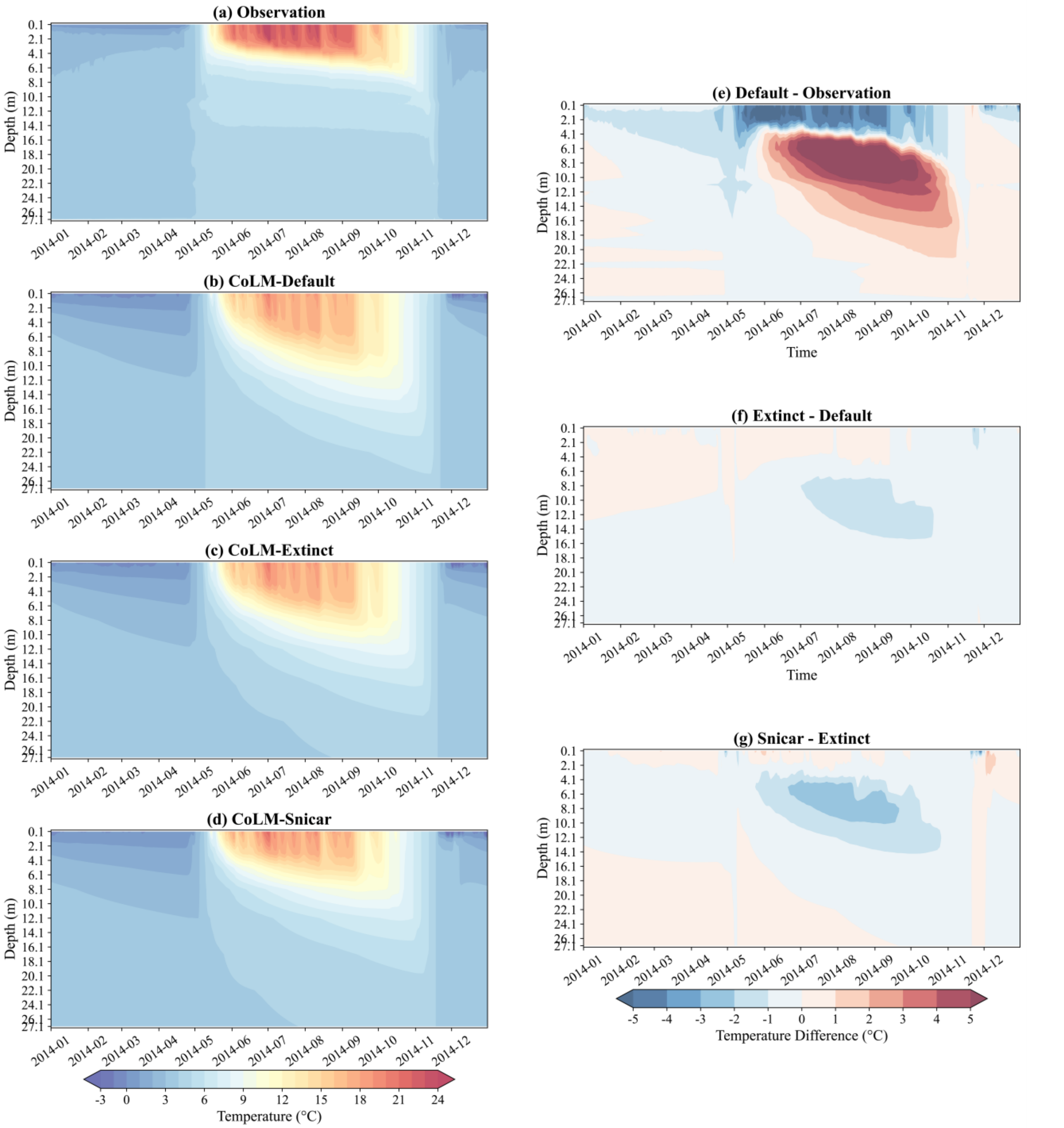

Figure 5. Same as Fig. 2 but for Lake Harp during 2014.

The depth-resolved statistics further identify the metalimnion as the most difficult layer to simulate (Fig. 6). Near the surface, all experiments retain high TCs because they well reproduce the seasonal warming and cooling cycle, although a cold bias

https://doi.org/10.5194/egusphere-2026-4210
Preprint. Discussion started: 22 July 2026

remains in the uppermost layers. The largest absolute errors occur at approximately 5-12 m, where the observed thermocline evolves seasonally. In this transition zone, CoLM-Default shows the strongest warm bias and the largest RMSE, consistent with the excessive downward heat penetration shown in Fig. 5e. CoLM-Extinct reduces this bias, but the bias and RMSE peaks remain evident. CoLM-Snicar flattens the peak more substantially. Throughout much of the thermocline and upper hypolimnion, it produces the smallest bias and the lowest RMSE among the three experiments (Fig. 6b and 6c). The improvement is especially clear where the default model over-warms the metalimnion. Below about 12 m, the temperature bias and RMSE are relatively small in all experiments because the hypolimnion varies slowly with a large thermal inertia. TC, however, decreases in these deep layers, because the observed annual temperature range is small at these depths, and even modest timing differences in warming or cooling can substantially reduce the correlation coefficient. Even so, CoLM-Snicar maintains comparable or better skill than the other two experiments in the lower part of Lake Harp, with the TC value remaining above 0.8.

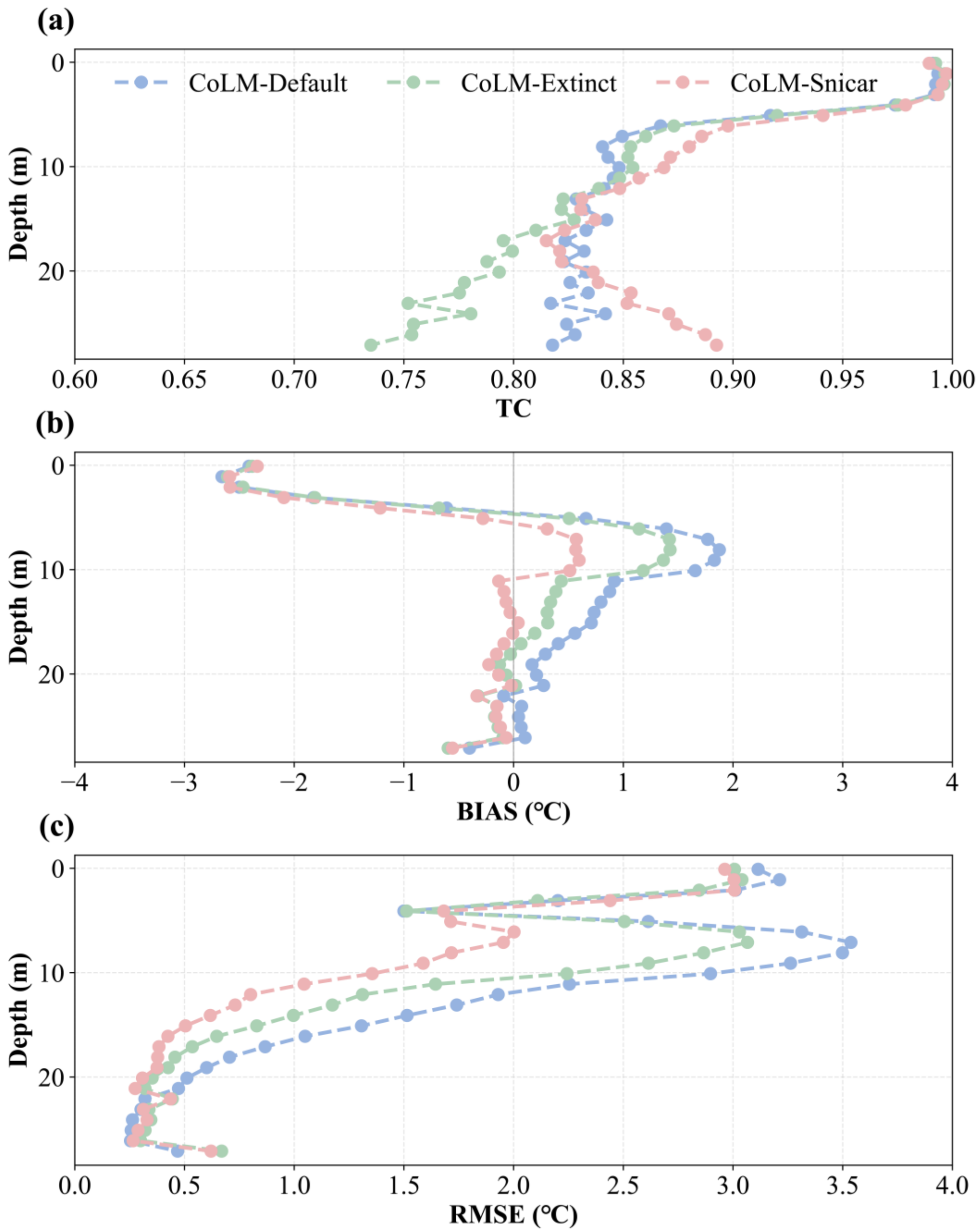

Figure 6. Same as Fig. 3 but for Lake Harp during 2014.

The comparison of the layer-by-layer solar energy absorption reveals the radiative mechanism behind the improved simulated thermal structure of Lake Harp (Fig. 7). As in Lake Crystal Bog, CoLM-Snicar permits part of the incident radiation to be absorbed within the snow and ice layers instead of forcing all shortwave energy into the top layer during the frozen periods. Thus, the upper water can obtain a portion of radiation, especially for bare-ice periods given the lower scattering and higher

https://doi.org/10.5194/egusphere-2026-4210
Preprint. Discussion started: 22 July 2026

transparency of lake ice compared to snow cover. During the open-water season, the upward redistribution of absorbed solar radiation occurs again as seen in Lake Crystal Bog. Relative to CoLM-Extinct, CoLM-Snicar increases absorption in the uppermost water layers, with the diffuse component showing the strongest enhancement, commonly about 8-15 W m^{-2} (Fig. 7f). At the same time, the absorption is reduced over the intermediate depths where the default and extinction-only schemes tend to deposit too much heat (Fig. 7e and 7f). This pattern provides a direct process-level explanation for the temperature differences in Fig. 5g: more solar energy is retained near the surface while less energy reaches the metalimnion and upper hypolimnion in CoLM-Snicar. The resulting heat redistribution strengthens the vertical temperature gradient and suppresses the excessive deepening of the simulated mixed layer in the other two experiments. In addition, Fig. S4 shows that CoLM-Snicar absorbs more total shortwave radiation than CoLM-Extinct during the open-water season, which further confirms that the summer cooling below the thermocline in CoLM-Snicar results from the vertical redistribution of solar energy absorption rather than the changes of total available radiation for the whole lake column.

https://doi.org/10.5194/egusphere-2026-4210
Preprint. Discussion started: 22 July 2026

Figure 7. Same as Fig. 4 but for Lake Harp during 2014.

Taken together, Figs. 5-7 show that for Lake Harp, the upgrade of the radiative transfer scheme mainly improves the dynamically active part of the water column, namely the mixed layer and metalimnion. These layers are crucial to lake-atmosphere coupling because biases in the evolution of mixed layer and thermocline depth affect the strength of stratification, the timing of overturn, and eventually the seasonal surface heat storage and release.

The other medium-depth lakes listed in Table 1 generally show responses to the new radiative transfer scheme consistent with those identified for Lake Harp. In Lake Trout Bog, CoLM-Snicar cools the metalimnion and upper hypolimnion relative to CoLM-Extinct and better constrains the thickness of the warm mixed layer, and thus improves the simulated vertical thermal structure (Figs. S5). In Lake Ngoring, CoLM-Snicar reproduces the under-ice warming by allowing shortwave radiation to penetrate through lake ice and warm the upper water layers, which markedly corrects the cold biases in CoLM-Default and

https://doi.org/10.5194/egusphere-2026-4210
Preprint. Discussion started: 22 July 2026

CoLM-Extinct (Figs. S6). Lake Trout is the only counterexample. At this site, the observed thermal structure is characterized by a relatively deep mixed layer and thermocline, whereas CoLM-Default and CoLM-Extinct already underestimate their depths (Fig. S7). By shifting a larger fraction of absorbed solar energy toward the upper water layers, CoLM-Snicar further shoals the simulated thermocline and cools the mid-depth layers relative to CoLM-Extinct, which increases the mismatch with observed temperatures. Therefore, for moderately deep lakes, the benefit of the spectral two-stream radiative-transfer treatment is largest when the original model deposits excessive summer heat below the mixed layer. Its advantage can be reduced, or even reversed, when the dominant error is the mid-depth cold bias arising from, for example, insufficient vertical mixing or entrainment. These results indicate that the broader applicability of CoLM-Snicar depends on joint improvements of radiation transfer and other model physics.

4.3 Model performances for the deep lake (Nam Co)

Lake Nam Co is used to evaluate the model in a deep, optically clear lake with a prescribed depth of 92 m and an observed water extinction coefficient of 0.08 m-1. In this lake, realistic simulation requires substantial seasonal heat storage below the surface layer. Therefore, it is worthwhile to test whether the upward redistribution of absorbed solar energy, which has been identified as the main effect of SNICAR-ADv5 on shortwave radiative transfer in those shallow and medium-depth lakes, can still improve the simulated vertical thermal structure for this deep and clear lake.

The observations of Lake Nam Co show a deep seasonal thermal response rather than a shallow, surface-confined stratification (Fig. 8a). Strong warming develops in the upper water layers during summer, and progressively penetrates to depths of several tens of meters by autumn. CoLM-Default captures the broad timing of surface warming, but it fails to reproduce the downward propagation of heat. During July-November, CoLM-Default underestimates the depth of the seasonal mixed layer and thermocline, resulting in a pronounced cold bias in the intermediate water column, with the largest bias centered at approximately 20-60 m (Figs. 8b and 8e). In contrast, during winter and spring, it becomes too warm over much of the water column. Introducing the site-specific water extinction coefficient in CoLM-Extinct significantly modifies the simulated thermal structure during the stratified warming season. Because the observed extinction coefficient is much smaller than the empirical value used in CoLM-Default, a larger fraction of shortwave radiation penetrates below the near-surface layers, warming the middle and deep water by approximately 1-3 °C and thereby reducing the summer-autumn cold bias (Figs. 8c and 8f).

CoLM-Snicar produces a more seasonally dependent response in Lake Nam Co. During winter and spring, it reduces the excessive warm bias simulated by CoLM-Default and CoLM-Extinct, particularly below approximately 20 m (Figs. 8d and 8g). This improvement can be attributed to the higher effective lake-system albedo simulated by CoLM-Snicar under snow- and ice-covered conditions, which decreases the total shortwave energy available to the entire lake column relative to the other two experiments (Fig. S8). As a result, the original over-warmed deep water is cooled, leading to a more realistic winter-spring thermal structure. During July-November, CoLM-Snicar also alleviates part of the cold bias in CoLM-Default. However, comparison with CoLM-Extinct reveals an important limitation. Relative to CoLM-Extinct, CoLM-Snicar produces a

https://doi.org/10.5194/egusphere-2026-4210
Preprint. Discussion started: 22 July 2026

shallower mixed layer and thermocline, and tends to cool the middle and deep layers by approximately 0.5-2.0 °C (Figs. 8d and 8g). This cooling partly offsets the deep-water warming in CoLM-Extinct that helps reduce the original summer-autumn cold bias. Thus, compared with CoLM-Extinct, CoLM-Snicar improves the seasonal and vertical heat distribution during winter and spring, but degrades the model skill during the stratified warming season. The latter result is similar to that found in Lake Trout, where the observed mixed layer and thermocline are also relatively deep but are underestimated by CoLM-Default and CoLM-Extinct, and CoLM-Snicar increases the thermal biases by the upward redistribution of absorbed shortwave radiation (Fig. S7).

https://doi.org/10.5194/egusphere-2026-4210
Preprint. Discussion started: 22 July 2026

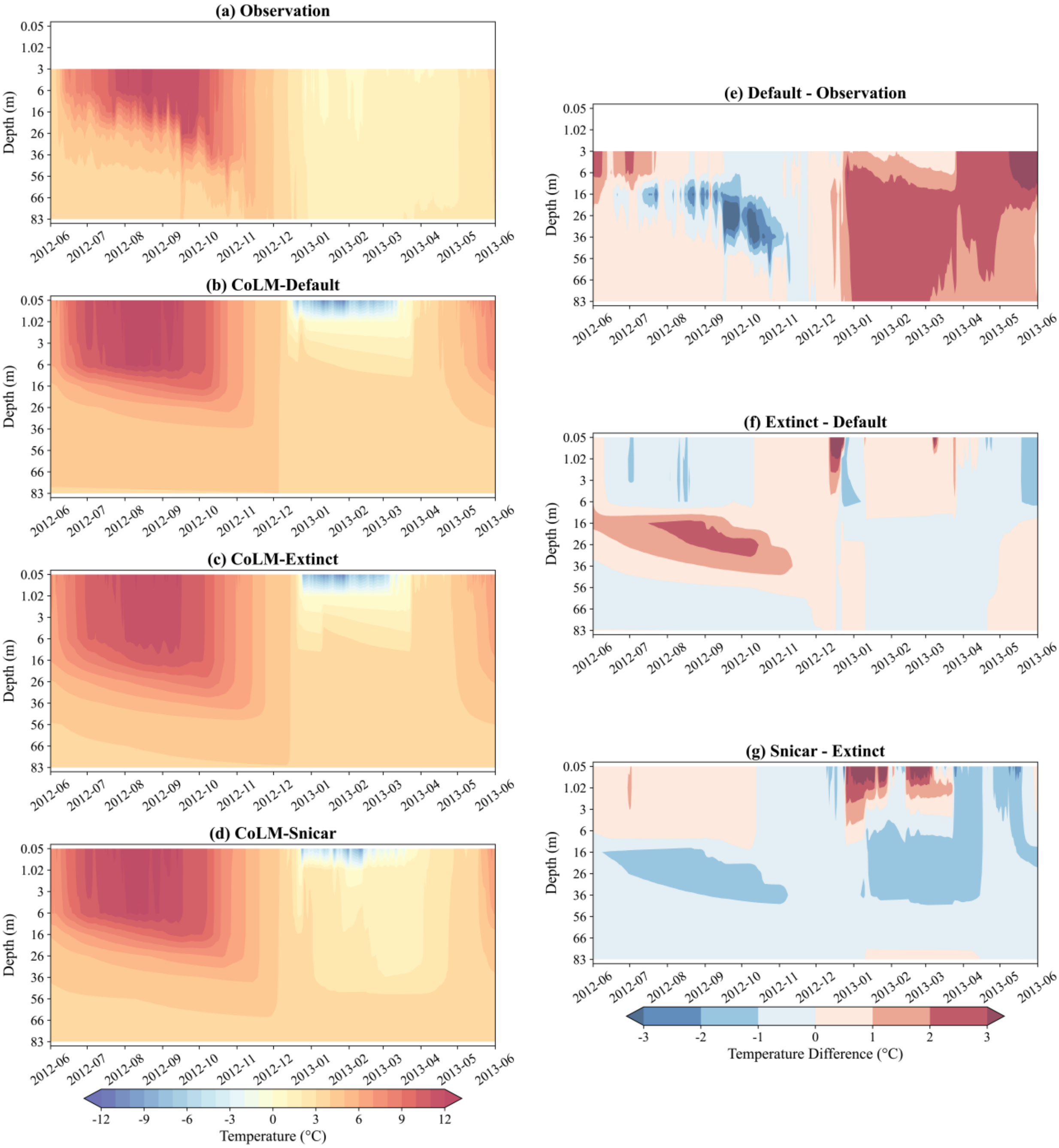

Figure 8. Same as Fig. 2 but for Lake Nam Co during 2012-2013.

The depth-resolved statistics further summarize the net performance of the three experiments in Lake Nam Co (Fig. 9). All simulations reproduce the seasonal timing of water-temperature variations reasonably well, with TC values generally exceeding 0.85 throughout the measured water column (Fig. 9a). The main differences are reflected in bias and RMSE. When

https://doi.org/10.5194/egusphere-2026-4210
Preprint. Discussion started: 22 July 2026

averaged over the full evaluation period, CoLM-Default is dominated by warm biases at most depths, despite the summer-autumn cold bias identified in the intermediate water column in Fig. 8e. CoLM-Extinct does not consistently improve upon CoLM-Default because the enhanced shortwave penetration associated with the smaller observed extinction coefficient further increases the warm biases in parts of the upper and intermediate water column (Fig. 9b). In contrast, CoLM-Snicar substantially reduces the warm biases from the near-surface layer to approximately 50 m and yields the lowest RMSE over most measured depths (Figs. 9b and 9c). This statistical improvement is consistent with the temperature-profile differences shown in Fig. 8g, where CoLM-Snicar more effectively corrects the excessive winter-spring warm bias simulated by CoLM-Default and CoLM-Extinct. Below about 60 m, the differences among experiments become much smaller, suggesting that deep-water temperatures in Lake Nam Co are less sensitive to shortwave radiative transfer treatment.

https://doi.org/10.5194/egusphere-2026-4210
Preprint. Discussion started: 22 July 2026

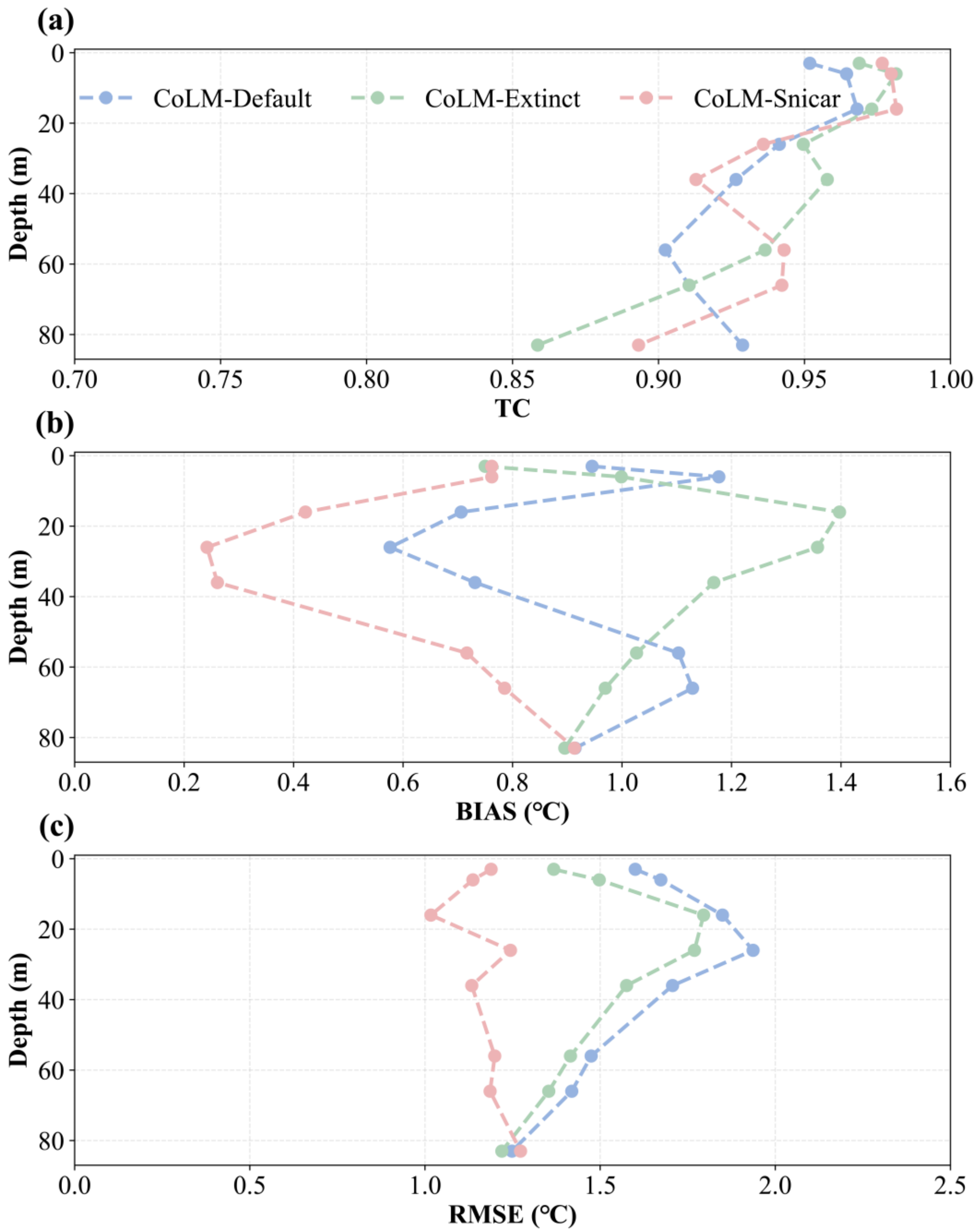

Figure 9. Same as Fig. 3 but for Lake Nam Co.

650 The layer-by-layer solar energy absorption in Lake Nam Co is compared in Fig. 10. The behaviors of CoLM-Snicar and CoLM-Extinct are broadly consistent with those identified for Lake Crystal Bog and Harp. During the ice-covered season, CoLM-Snicar permits part of the incident shortwave radiation, particularly the diffuse component, to penetrate the frozen surface layer and be absorbed in the upper and intermediate water layers, whereas CoLM-Extinct confines all shortwave absorption to the

https://doi.org/10.5194/egusphere-2026-4210
Preprint. Discussion started: 22 July 2026

uppermost frozen layer. During the open-water season, CoLM-Snicar redistributes absorbed shortwave energy upward relative to CoLM-Extinct, enhancing absorption in the upper water layers but reducing radiative heating below the thermocline, especially at depths of approximately 18-40 m. This upward redistribution increases near-surface energy acquisition but weakens the radiative supply to the depth range that contributes to seasonal heat storage, which thereby explains the enlarged cold biases of middle and deep layers in CoLM-Snicar compared to CoLM-Extinct (Fig. 8g). In shallow and most medium-depth lakes, a reduction in deep radiative deposition is beneficial because the original model tends to overheat the lower water column. In Lake Nam Co, however, the same mechanism can degrade the model performance because it limits the required heat storage below the thermocline unless other processes such as turbulent mixing, entrainment, and seasonal overturn transport sufficient heat downward.

Overall, Lake Nam Co highlights both the strengths and limitations of coupling SNICAR-ADv5 with CoLM-Lake. The explicit radiative-transfer treatment improves the simulated thermal structure in the upper and intermediate water column, and provides a more physically based representation of shortwave radiation transfer under snow- and ice-covered conditions. However, during the open-water season, CoLM-Snicar redistributes absorbed shortwave energy toward the upper water layers, thereby reducing radiative heating below the thermocline and potentially maintaining or amplifying the cold biases in the middle and deep water column. Together with the medium-depth lakes discussed above, Lake Nam Co delineates an important applicability boundary for the coupled model: improving radiative transfer can substantially alter the simulated lake thermal structure, but its net benefit remains lake dependent. In deep lakes, seasonal heat storage in the lower water column is jointly regulated by radiative penetration, vertical mixing, entrainment, and seasonal overturning, all of which are common sources of uncertainty in 1-D lake models (Dai et al., 2018; Gu et al., 2015; Huang et al., 2019; Subin et al., 2012). Therefore, the effect of improved shortwave radiative-transfer scheme should be interpreted in conjunction with the model's ability to represent these heat-storage and mixing-related processes.

https://doi.org/10.5194/egusphere-2026-4210
Preprint. Discussion started: 22 July 2026

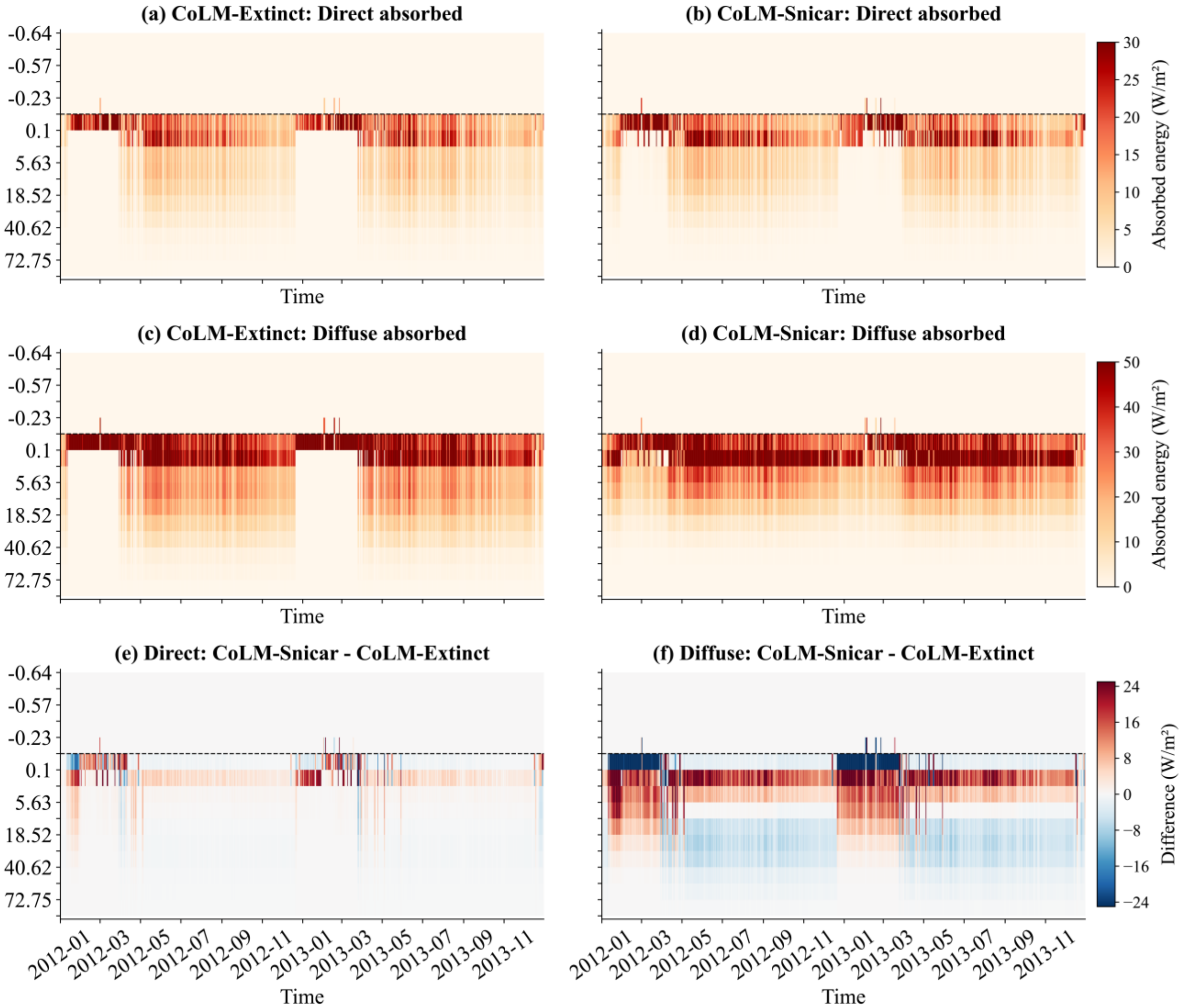

Figure 10. Same as Fig. 4 but for Lake Nam Co during 2012-2013.

4.4 Overall evaluations across all lakes

We next synthesize the model behaviors across all lakes. Figure 11 evaluates thermocline depth during open-water periods for the six lakes in which a thermocline can be diagnosed. Across these stratified lakes, CoLM-Snicar generally reduces the errors of thermocline depth when CoLM-Default or CoLM-Extinct places the thermocline too deep because of excessive radiative heat deposition below the mixed layer. This improvement is most evident in Lake Crystal Bog, Trout Bog, and Harp, where CoLM-Snicar substantially reduces both RRMSE and relative bias compared with CoLM-Default and CoLM-Extinct (Figs. 11a and 11b). For Lake Trout and Nam Co, CoLM-Snicar produces only small changes in RRMSE and relative bias, and even slightly increases the error magnitude in some cases. However, it yields the highest correlation, suggesting a better

https://doi.org/10.5194/egusphere-2026-4210
Preprint. Discussion started: 22 July 2026

representation of the seasonal timing of thermocline evolution (Fig. 11c). In addition, the lower correlation in Lake Harp indicates that reducing the mean bias of thermocline depth does not necessarily improve the timing of thermocline development and decay. These results are consistent with the process-level diagnostics presented in the above sections. During open-water periods, SNICAR-ADv5 tends to shift absorbed shortwave energy upward. This redistribution is beneficial when the original model deposits too much heat below the mixed layer, but it can be neutral or detrimental when the dominant error is instead associated with insufficient downward heat propagation.

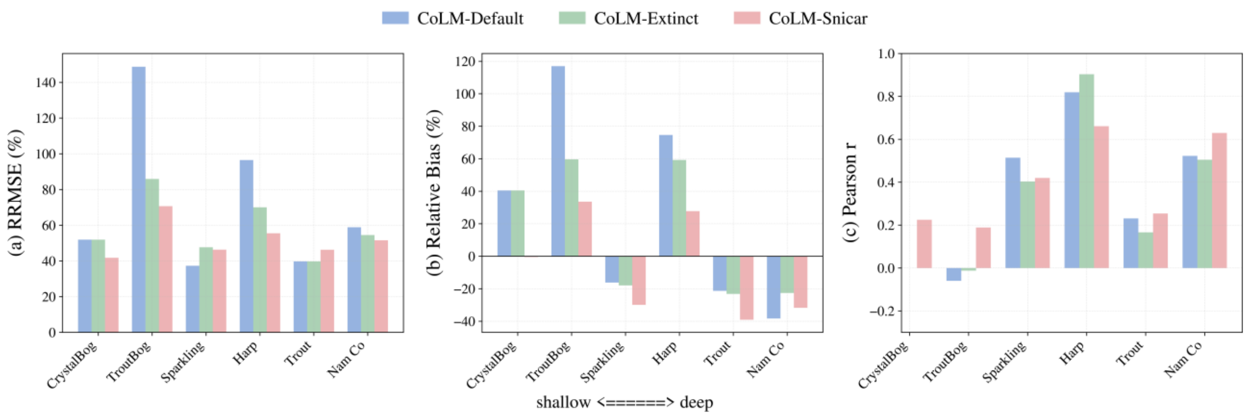

Figure 11. Performance statistics for simulated thermocline depth during open-water periods. (a) Relative root-mean-square error (RRMSE), (b) relative bias, and (c) Pearson correlation coefficient (r) for the three model experiments. Lakes are ordered from shallow to deep, and only lakes with a diagnosable thermocline in the observations are included. Note that the Pearson correlation coefficients for Lake Crystal Bog are not reported for CoLM-Default and CoLM-Extinct because these two experiments simulate a fully mixed water column during the evaluation period (Fig. 2b and 2c), preventing the temporal correlation of thermocline depth from being calculated.

To further separate errors in the actively mixed portion of the water column from those in the deeper heat-storage region, Fig. 12 summarizes the simulation skill by vertical zone for lakes with a diagnosed thermocline during open-water periods. In the upper water zone (the extent from the lake surface to the bottom of the thermocline), CoLM-Snicar gives consistent improvements in lakes where the above sections identify excessive downward heat penetration. It reduces RRMSE and relative bias in Lake Crystal Bog, Trout Bog, and Harp, and slightly increases the temporal correlation in these lakes (Fig. 12A). These changes indicate that the spectral two-stream treatment improves the timing and magnitude of mixed-layer warming by retaining a larger fraction of absorbed shortwave energy near the surface. The improvement is small or reversed in Lake Sparkling, Trout, and Nam Co, where the upper-layer biases are already modest or where the SNICAR-induced upward redistribution of solar radiation partly offsets the heat penetration required to sustain deeper seasonal warming. In the deep water zone (the region below the thermocline), the effect of CoLM-Snicar is also lake dependent but remains physically interpretable. CoLM-Snicar markedly reduces deep-water RRMSE and positive relative bias in Lake Crystal Bog, Trout Bog, Sparkling, and Harp (Fig. 12B1 and 12B2), consistent with the reduced solar energy deposition below the mixed layer.

https://doi.org/10.5194/egusphere-2026-4210
Preprint. Discussion started: 22 July 2026

However, the deep-zone correlation remains comparable among the three experiments, and is only moderately improved in Lake Crystal Bog by CoLM-Snicar (Fig. 12B3), which reflects the small seasonal temperature range and the strong sensitivity of correlation to phase errors in the hypolimnion. For Lake Trout and Nam Co, the deep-zone metrics show more limited benefit, again suggesting that radiative transfer alone cannot compensate for mixing or overturning errors in deep lakes.

The full-profile statistics integrate these vertical comparisons (Fig. 12C). CoLM-Snicar generally provides the lowest or comparable RRMSE and relative bias across most lakes, with particularly remarkable improvements in Lake Crystal Bog, Trout Bog, and Harp. The full-profile correlations are high for Lake Kossenblatter, Tai, Sparkling, Harp, Trout, and Nam Co, while the relatively lower values for Lake Crystal Bog and Trout Bog indicate that accurately capturing the timing of thermal transitions remains challenging. Overall, the multi-lake evaluation confirms the core result from the individual cases: improving shortwave radiative transfer strengthens the simulated mixed-layer and thermocline structure, but the net benefit depends on how radiative heating interacts with lake vertical mixing, depth, and optical conditions.

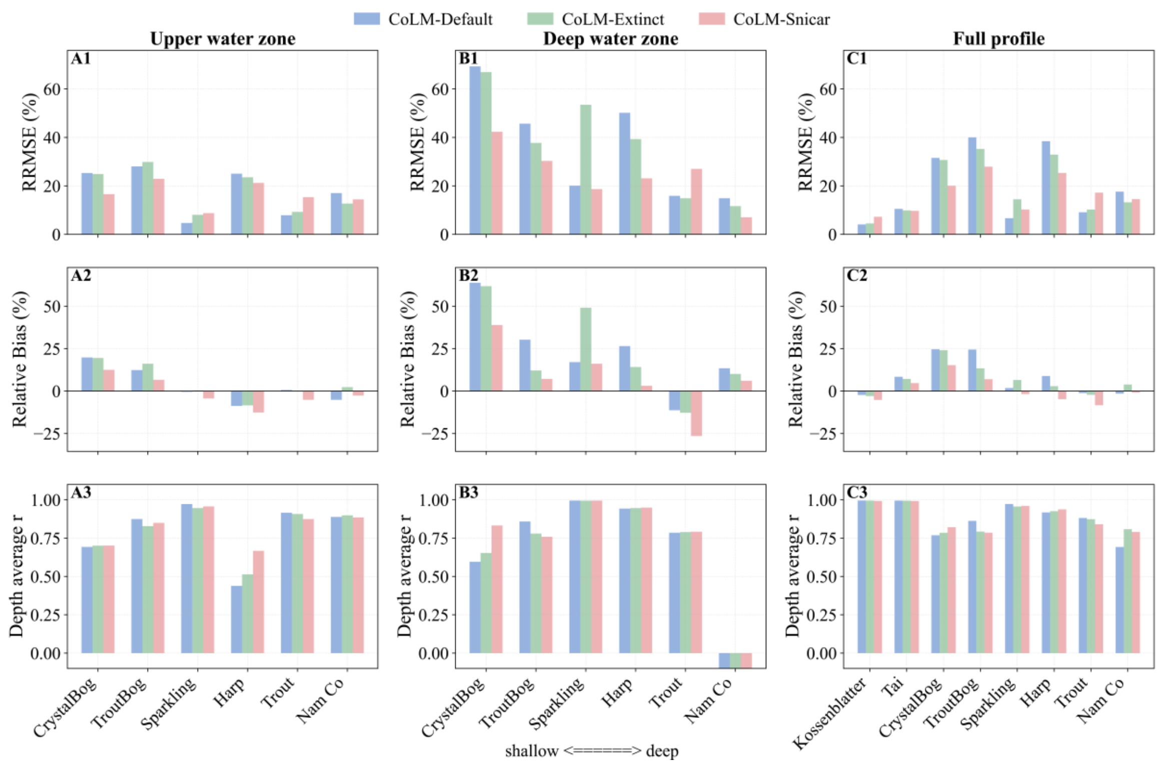

Figure 12. Vertical-zone evaluations of lake water temperature simulations during open-water periods. Metrics include RRMSE, relative bias, and Pearson correlation coefficient (r) for (A1-A3) the upper water zone, (B1-B3) the deep water zone, and (C1-C3) the full measured water column. For thermally stratified lakes, the upper water zone extends from the lake surface to the bottom of the thermocline, and the deep water zone includes the remaining layers below. For Lake Kossenblatter and Tai, where no persistent thermocline is diagnosed, only full-profile statistics over the entire simulation period are reported.

https://doi.org/10.5194/egusphere-2026-4210
Preprint. Discussion started: 22 July 2026

4.5 Evaluation of Lake Ice Phenology

Fig. 13 and Table 2 summarize the simulated seasonal evolution of lake-ice thickness and the corresponding freeze-up (ice-on) and break-up (ice-off) dates for the lakes whose simulation periods include a complete ice freeze-thaw cycle. Because SNICAR-ADv5 explicitly partitions shortwave radiation among snow, ice, and water, it affects lake-ice evolution by changing the balance between solar energy absorbed within the ice and energy transmitted to the underlying water.

Freeze-up timing is controlled mainly by autumn surface cooling and by the heat content of water layers that remain coupled to the surface during pre-freeze overturning. For Lake Crystal Bog, Trout Bog, Trout, and Ngoring, the simulated ice-on dates are generally similar among the three experiments, although all configurations simulate freeze-up in Lake Ngoring approximately 16 days earlier than observed. Larger inter-experiment differences occur in Lake Harp and Nam Co. Relative to CoLM-Extinct, CoLM-Snicar advances ice-on in Lake Harp by about 6 days but delays ice-on in Lake Nam Co by 8 days. These opposite responses are consistent with the corresponding pre-winter near-surface thermal states: CoLM-Snicar produces surface cooling in Lake Harp, which facilitates earlier ice formation, but surface warming in Lake Nam Co, which increases the amount of heat that must be removed before freeze-up can occur (Figs. 5g and 8g).

The simulated ice-thickness curves further show that the radiative transfer treatment affects ice mass balance throughout the frozen season. In Lake Harp, Ngoring, and Nam Co, CoLM-Snicar generally maintains thinner ice than the other two experiments, indicating that the transmission of part of the shortwave radiation through the ice can increase under-ice energy availability and inhibit ice growth. In Lake Crystal Bog, Trout Bog, and Trout, the differences in ice thickness among the three experiments are relatively modest.

During the ablation season, the impact of SNICAR-ADv5 on ice-off timing becomes more evident. For the North American lakes with observed ice phenology, CoLM-Snicar delays ice-off by 1-7 days relative to CoLM-Default and CoLM-Extinct, thereby reducing the large early break-up bias, although break-up is still simulated too early. In Lake Nam Co, CoLM-Snicar delays ice-off even more substantially, by 16 days relative to the other two experiments. In contrast, CoLM-Snicar advances ice-off in Lake Ngoring by nearly 20 days, shifting the bias from late to early. These contrasting responses are consistent with the differences in simulated total shortwave energy absorbed by the lake system during the ice-covered season. In most lakes, CoLM-Snicar reduces total absorbed shortwave energy relative to CoLM-Extinct, as illustrated for Lake Harp and Lake Nam Co (Figs. S4 and S8). Under these conditions, although part of incident radiation is allowed to penetrate through the ice and heat the underlying water, the resulting under-ice warming is insufficient to compensate for the reduced radiative energy absorbed within the ice layer. The net effect is therefore slower spring ablation and a longer ice-cover duration. Lake Ngoring represents the opposite case. CoLM-Snicar increases total absorbed shortwave energy relative to CoLM-Extinct in Lake Ngoring (Fig. S9), and the transmitted radiation supplies sufficient energy to the under-ice water, which produces pronounced warming beneath the ice (Fig. S6g) and enhances basal melt. This mechanism plausibly explains why CoLM-Snicar advances ice-off date in Lake Ngoring while delaying break-up in the other ice-covered lakes. This mechanism is further discussed in Section 5.2.

https://doi.org/10.5194/egusphere-2026-4210
Preprint. Discussion started: 22 July 2026

Overall, the lake-ice simulations show that explicitly resolving snow-ice-water radiative transfer improves the simulated lake ice phenology, and significantly changes lake ice thickness. The direction and magnitude of the response depend on lake-specific optical and thermal conditions. The same radiative redistribution can either reduce energy absorption within ice layers and delay break-up, or enhance under-ice water heating and accelerate basal melt. These results demonstrate that physically based radiative-transfer treatments are essential for lake-ice modeling, while their net effect must be interpreted together with snow cover, ice optical properties, water clarity, and the efficiency of heat transfer at the ice-water interface.

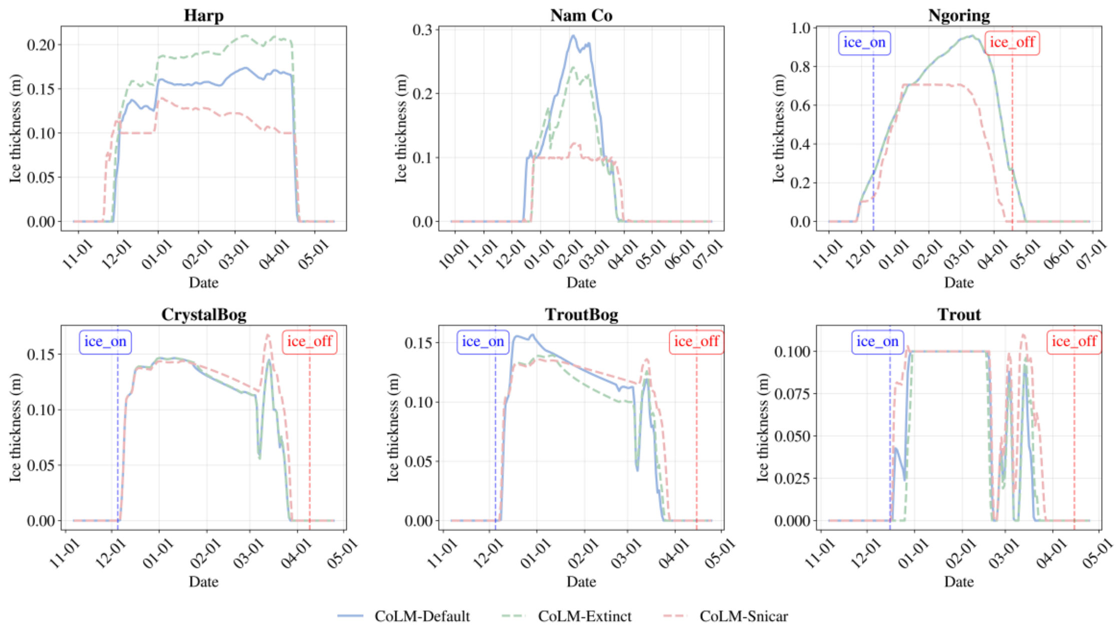

Figure 13. Simulated seasonal evolution of lake-ice thickness under the three model experiments. Vertical blue dashed lines mark observed freeze-up (ice-on) dates, and vertical red dashed lines mark observed break-up (ice-off) dates where observations are available.

Table 2. Observed and simulated freeze-up (ice-on) and break-up (ice-off) dates for lakes with seasonal ice. NA indicates that the corresponding observational date is not available.

Lake	Ice state	Observation	CoLM-Default	CoLM-Extinct	CoLM-Snicar
Harp	Ice on	NA	2014-11-27	2014-11-26	2014-11-20
	Ice off	NA	2015-04-26	2015-04-26	2015-04-26
Nam Co	Ice on	NA	2012-12-13	2012-12-21	2012-12-29
	Ice off	NA	2013-04-09	2013-04-09	2013-04-25
Ngoring	Ice on	2015-12-12	2015-11-26	2015-11-26	2015-11-26
	Ice off	2016-04-18	2016-05-02	2016-05-02	2016-04-12

https://doi.org/10.5194/egusphere-2026-4210
Preprint. Discussion started: 22 July 2026

Crystal Bog	Ice on	2016-12-05	2016-12-06	2016-12-06	2016-12-06
	Ice off	2017-04-09	2017-03-27	2017-03-27	2017-03-28
Trout Bog	Ice on	2016-12-05	2016-12-08	2016-12-08	2016-12-08
	Ice off	2017-04-15	2017-03-24	2017-03-25	2017-03-28
Trout	Ice on	2016-12-16	2016-12-17	2016-12-25	2016-12-17
	Ice off	2017-04-15	2017-03-20	2017-03-23	2017-03-27

5 Discussion

5.1 Mechanisms for vertical distribution of shortwave radiation absorption in CoLM-Lake coupled with SNICAR-ADv5 during open-water periods

The results in Section 4 show that the primary effect of coupling SNICAR-ADv5 with CoLM-Lake is not simply to increase or decrease the total amount of solar energy absorbed by the lake system, but to redistribute the absorbed energy vertically. This distinction is central to understanding the model response during open-water periods. Shortwave absorption acts as a depth-dependent heat source. Energy absorbed within the surface mixed layer enhances near-surface warming, increases buoyancy, strengthens stratification, and can suppress entrainment across the thermocline. In contrast, energy absorbed below the mixed layer increases subsurface heat storage, weakens vertical temperature gradients, and affects the timing and magnitude of seasonal heat release. Thus, the vertical distribution of radiative heating is a key control on lake thermal evolution.
The difference between CoLM-Snicar and the other two experiments arises from how the radiation field is represented within the lake column. In CoLM-Default, direct and diffuse shortwave radiation are treated differently at the air-water interface: during open-water periods, the effective direct-beam albedo depends on solar zenith angle, whereas diffuse albedo is prescribed as a constant. However, once radiation enters the water column, the penetrating component is distributed using the same single-band Beer-Lambert attenuation profile, which implicitly treats underwater radiation as a vertically downward propagating flux. As a result, the original scheme retains only a bulk extinction scale and does not allow the subsurface absorption profile to respond to illumination geometry, spectral composition, scattering, or internal reflection. CoLM-Extinct improves this framework by replacing the empirical depth-dependent extinction coefficient with an observation-based value, a correction that is particularly effective in highly turbid lakes such as Lake Tai and Kossenblatter. Nevertheless, it does not remove the structural limitation that all penetrating radiation follows one prescribed exponential decay profile.

By contrast, SNICAR-ADv5 represents shortwave transfer as a spectral two-stream problem in a layered medium. In CoLM-Snicar, direct and diffuse radiation are treated separately after entering the water column, and absorption is determined by wavelength-dependent optical properties, scattering, Fresnel reflection and transmission, and repeated radiative interactions among layers (Tolento et al., 2024). This treatment allows the effective optical path length to differ from the vertical depth interval. For direct radiation, the incident angle and refraction at the air-water interface produce a slant propagation path in

https://doi.org/10.5194/egusphere-2026-4210
Preprint. Discussion started: 22 July 2026

water. When solar elevation is low, the direct beam travels a longer optical path for the same vertical displacement, which increases the probability of absorption in the upper layers. Diffuse radiation has an even broader range of propagation directions because it enters from the downward hemisphere rather than from a single beam direction. Its mean underwater path is therefore generally more oblique than that of a near-normal direct beam. This geometric effect promotes shallower shortwave absorption, especially for the diffuse component as shown in Figs. 4, 7, and 10.

Scattering further reinforces this upward redistribution of absorbed energy in CoLM-Snicar. In the two-stream solution, part of the direct beam is converted into diffuse radiation, and upward and downward fluxes are coupled through scattering and internal reflection (Tolento et al., 2024). Meanwhile, the adding-doubling algorithm allows radiation to be repeatedly reflected and transmitted between adjacent layers before absorption (Briegleb and Light, 2007), thereby increasing photon residence time and modifying the effective absorption depth. Therefore, even when column-integrated absorption changes only modestly or decreases, the increase in effective photon path length can shift absorbed energy from deeper water toward the near-surface layers. This mechanism explains why CoLM-Snicar consistently increases absorption in the upper water column and reduces absorption below the mixed layer during open-water periods.

The thermal consequences of this radiative redistribution depend on lake depth, water clarity, and the dominant source of model errors. In shallow and moderately deep lakes where CoLM-Default and CoLM-Extinct tend to deposit excessive heat below the mixed layer, the SNICAR-induced upward shift in absorption improves the simulated thermal structure. Lake Crystal Bog, Harp, and Trout Bog are representative examples, demonstrating that a more physically based vertical heating profile can reduce unrealistic downward solar heat penetration in many seasonally stratified lakes. However, the same mechanism can become neutral or even detrimental when the original model already underestimates downward heat propagation. This behavior is evident in Lake Trout, Sparkling, and Nam Co, where the observed thermal structure requires substantial seasonal heat storage beneath the near-surface layer. By shifting more absorbed solar energy upward and reducing radiative heating below the thermocline, CoLM-Snicar can intensify mid-depth cold biases if vertical mixing, entrainment, or seasonal overturning does not transport sufficient heat downward. These results do not imply that the spectral two-stream treatment is less physical in such cases. Rather, they show that improved radiative transfer can expose remaining limitations in other components of 1-D lake models, particularly the representation of vertical mixing and deep heat storage. In addition, CoLM-Default exhibits a pronounced warm bias near the lake bottom of Sparkling (Fig. S10e), which may partly reflect the influence of relatively strong groundwater inflow that supplies cold water to the hypolimnion during summer (Webster et al., 1996). Such groundwater exchange beneath the lake bed is not represented in CoLM-Lake. Although CoLM-Snicar reduces the deep-water warm bias by limiting excessive radiative heating below the mixed layer, it does not fully eliminate the bias (Fig. S10g). This remaining error suggests that, in addition to radiative transfer and vertical mixing, lake hydrological processes such as groundwater inflow may also need to be represented for lake systems.

Overall, CoLM-Snicar provides a more physically consistent representation of shortwave absorption by accounting for illumination geometry, spectral dependence, scattering, and interfacial radiative exchange during open-water periods. Its most robust process-level signature is a shallower distribution of absorbed solar energy relative to the original Beer-Lambert-based

https://doi.org/10.5194/egusphere-2026-4210
Preprint. Discussion started: 22 July 2026

treatment, particularly for diffuse radiation. This redistribution improves simulations when excessive deep radiative heating is the dominant error, but its net impact depends on how radiative heating interacts with lake-specific optical properties and with the model representation of other physics such as turbulent mixing, entrainment, and overturning. The coupled CoLM-Lake and SNICAR-ADv5 framework can therefore serve not only as an upgraded radiative-transfer scheme, but also as a diagnostic tool for identifying whether lake thermal biases arise primarily from radiation, mixing, or their interaction.

5.2 Impacts of SNICAR-ADv5 on lake ice phenology in CoLM-Lake

The influence of SNICAR-ADv5 on lake-ice phenology can be interpreted as a change in the seasonal heat-budget pathways of the snow-ice-water column. In CoLM-Default and CoLM-Extinct, the frozen lake surface is treated as an optically opaque absorber. After surface reflection is removed, the remaining shortwave radiation is deposited in the uppermost snow or ice layer. This treatment may occasionally reproduce an observed freeze-up or break-up date, but it cannot resolve how solar energy is partitioned among reflection to the atmosphere, absorption within snow and ice, transmission to the underlying water, and subsequent heat storage beneath the ice. By explicitly representing spectral absorption, scattering, Fresnel reflection, and transmission, CoLM-Snicar introduces these missing pathways and allows lake-ice phenology to emerge from the coupled effects of radiation, heat conduction, phase change, and under-ice water heat storage (Kirillin et al., 2012; Oveisy and Boegman, 2014).

Different radiative pathways have different thermodynamic consequences. Shortwave absorption within the ice can enhance internal heating, affect conductive ice growth, and promote internal or surface melt (W. Huang et al., 2022; Oveisy and Boegman, 2014). In contrast, radiation transmitted through the ice and absorbed in the underlying water can build an under-ice heat reservoir, enhance basal melting, and trigger convective mixing when solar heating drives water temperature toward the temperature of maximum density (W. Huang et al., 2022; Kirillin et al., 2021; Lazhu et al., 2021; M. Wang et al., 2022). These under-ice processes are largely inaccessible to an opaque-ice approximation, but they become physically interpretable when snow, ice, and water are treated as a radiatively active column.

Snow cover acts as an important optical regulator of shortwave transmission through the frozen lake surface. Even a thin snow layer can increase surface albedo and strongly attenuate shortwave radiation before it reaches the ice or water layers (W. Huang et al., 2022; Weyhenmeyer et al., 2022), as shown for Lake Crystal Bog and Harp (Figs. 4 and 7). In contrast, snow-free or weakly snow-covered conditions allow a larger fraction of shortwave radiation to enter the ice. The ice layer further filters this transmitted radiation, and its effect depends strongly on ice optical and microphysical properties. Clear black or blue ice with relatively low bubble and impurity content can transmit a substantial fraction of shortwave radiation to the water below, whereas white ice, bubble-rich ice, or impurity-contaminated ice enhances scattering and internal absorption, thereby reducing the energy reaching the under-ice water (W. Huang et al., 2022; Kirillin et al., 2021; M. Wang et al., 2022; Weyhenmeyer et al., 2022). Thus, the same incident solar forcing can produce different melt pathways depending on whether energy is absorbed within the ice or transmitted into the water column. This sensitivity explains why lake-specific ice optical and microphysical properties are critical for evaluating the effects of the coupled model.

https://doi.org/10.5194/egusphere-2026-4210
Preprint. Discussion started: 22 July 2026

The ice freeze-up response reflects the combined effects of open-water heat storage, autumn cooling, and the reconnection of subsurface heat anomalies to the surface during overturn (Kirillin et al., 2017; Z. Li et al., 2021; Ma et al., 2022; Zhou et al., 2023). A more surface-concentrated radiative heating profile during the open-water period can delay ice formation if the warmed mixed layer retains sufficient heat into late autumn. Conversely, it can advance freeze-up if this near-surface heat is rapidly lost to the atmosphere and the reduced subsurface heat storage leaves less energy available to sustain surface temperatures. This mechanism helps explain the contrasting freeze-up responses in Lake Nam Co and Harp among the three experiments. In deep, optically clear Lake Nam Co, CoLM-Snicar increases shortwave absorption in the upper and intermediate water layers relative to the other experiments during the open-water season (Figs. 10e and 10f). Since the effective mixed layer is relatively thick, part of this additional heat can persist into the pre-freeze period and maintain a warmer surface layer (Fig. 8g). At the same time, the SNICAR-induced reduction in deeper heat storage has a weaker immediate influence on freeze-up, because this deep cold anomaly is less efficiently communicated to the surface before ice-on during the limited pre-freeze mixing period (Lazhu et al., 2016; Ma et al., 2022; Zhou et al., 2023). Together, these effects make it more difficult for the surface water to reach the freezing point in CoLM-Snicar, thereby delaying ice-on. In medium-depth Lake Harp, by contrast, the additional near-surface heat introduced by SNICAR-ADv5 is confined to a shallower layer (Figs. 7e and 7f), and thus can be dissipated more efficiently through lake-atmosphere heat exchange during autumn atmospheric cooling (Heiskanen et al., 2015). Meanwhile, the reduced heat storage in the relatively shallow metalimnion and upper hypolimnion is more likely to be mixed back toward the surface during autumn overturn (Heiskanen et al., 2015; Tan et al., 2018). These effects can accelerate surface heat loss and favor earlier ice formation in CoLM-Snicar. The above analyses suggest that differences in freeze-up timing do not arise from radiative transfer alone, but also from how radiative heating interacts with lake depth, mixed-layer evolution, autumn overturn, and pre-freeze heat storage.

Ice break-up is regulated by the balance between reduced shortwave absorption within the ice and enhanced basal melt driven by under-ice warming from ice-transmitted radiation (W. Huang et al., 2022; Kirillin et al., 2021; Z. Li et al., 2021; M. Wang et al., 2022). If the SNICAR-induced reduction in solar energy absorbed by the ice is not compensated by sufficient under-ice warming, the ice cover can persist longer. Conversely, if a substantial fraction of radiation penetrates through the ice and is absorbed near the ice-water interface, the resulting under-ice warming can enhance basal melt and accelerate break-up. This balance explains the contrasting break-up responses in Lake Nam Co and Ngoring among the three experiments. In Lake Nam Co, CoLM-Snicar produces a higher effective frozen-surface albedo and lower total shortwave absorption than the other experiments during the ice-covered season (Fig. S8). As a result, less shortwave radiation is available for transmission through the ice and absorption by the underlying water. In addition, the transmitted radiation is distributed over a deep and optically clear water column with a large heat capacity, making under-ice warming weaker than in shallower or more turbid lakes. Therefore, the reduced shortwave absorption within the ice cannot be fully compensated by under-ice warming, and the simulated break-up is delayed relative to CoLM-Default and CoLM-Extinct. The higher frozen-surface albedo simulated by CoLM-Snicar is likely related to the presence of a thin layer of snow cover or white ice, both of which can substantially increase reflection and limit solar penetration (W. Huang et al., 2022; Z. Li et al., 2021; Weyhenmeyer et al., 2022). Lake

https://doi.org/10.5194/egusphere-2026-4210
Preprint. Discussion started: 22 July 2026

Ngoring shows the opposite response. CoLM-Snicar simulates a lower effective frozen-surface albedo and greater total shortwave absorption during the ice-covered season (Fig. S9). This result is consistent with Wang et al. (2022), who adopted an effective frozen-surface albedo of 0.25 with a snow-free condition, much lower than the prescribed visible and near-infrared ice albedos of 0.6 and 0.4 used in the original CoLM-Lake scheme. By reducing this high-albedo bias, CoLM-Snicar allows more shortwave energy to enter the lake system and increases the radiative energy available to the under-ice water. Moreover, Lake Ngoring is shallower and less optically clear than Lake Nam Co (Table 1), so the transmitted radiation is absorbed within a smaller under-ice water volume and closer to the ice-water interface. The resulting stronger under-ice warming enhances basal melt and advances the simulated ice-off date. These mechanisms clarify the broader significance of coupling SNICAR-ADv5 with CoLM-Lake. A lake model may reproduce an observed break-up date for the wrong reason if it melts an opaque surface layer without representing the under-ice heat reservoir that develops beneath transparent ice. This issue is especially important for high-elevation or arid-region lakes, where limited snow cover and strong solar radiation can make under-ice radiative heating a major control on winter thermal structure and spring melt (W. Huang et al., 2022; Kirillin et al., 2021; Lazhu et al., 2021; M. Wang et al., 2022). CoLM-Snicar reduces this ambiguity by separating the locations of shortwave absorption and by allowing ice phenology to respond to physically distinct melt pathways. Future improvements should therefore treat snow-ice optical properties, ice thermodynamics, and under-ice heating and mixing as coupled processes rather than independent parameterizations (Rooney and Jones, 2010; Subin et al., 2012).

5.3 The applicability and uncertainties of CoLM-Lake coupled with SNICAR-Adv5

The mechanisms discussed above indicate that coupling CoLM-Lake with SNICAR-ADv5 should be interpreted as a physically based radiative-transfer upgrade rather than as a universally error-reducing calibration. Its primary applicability lies in lakes where CoLM-Lake biases are mainly caused by overly simplified shortwave absorption profiles, especially shallow and moderately deep lakes in which the default Beer-Lambert treatment deposits excessive solar energy below the mixed layer. In these cases, the spectral two-stream solution, explicit scattering, and interfacial reflection and transmission represented by SNICAR-ADv5 produce a shallower and more realistic radiative-heating profile, thereby improving mixed-layer thickness, thermocline depth, and hypolimnetic temperature. This behavior is consistent with previous lake-model studies showing that light extinction and water clarity are first-order controls on stratification, lake-atmosphere heat exchange, and ice phenology (M. Guo et al., 2021; Heiskanen et al., 2015). The coupled model is therefore particularly useful for physical-process studies and land-model applications in which the accurate vertical distribution of shortwave radiative heating controls the lake thermal response.

The coupled model is also well suited for seasonally ice-covered lakes where transparent ice or weak snow cover allows solar radiation to penetrate into the water column. Traditional opaque-ice and opaque-snow treatments force all non-reflected shortwave energy to be absorbed near the uppermost surface layer. In contrast, CoLM-Snicar separates shortwave absorption within snow, ice, and water, and therefore provides a more physically interpretable framework for diagnosing internal ice heating, under-ice water warming, basal melt, and the lengthening or shortening of ice-cover duration. In this sense, coupling

https://doi.org/10.5194/egusphere-2026-4210
Preprint. Discussion started: 22 July 2026

SNICAR-ADv5 extends CoLM-Lake from a thermodynamic lake model with prescribed radiative assumptions toward an optically active snow-ice-water integrated model that can better distinguish competing melt pathways.

However, the results also identify an important applicability boundary of the coupled model. In lakes that require strong downward heat transport, particularly deep or optically clear lakes, the more physically constrained radiative transfer scheme may expose deficiencies in the host lake model rather than eliminate the simulated temperature biases. The cases of Lake Trout and Nam Co illustrate this behavior. By shifting absorbed shortwave energy toward the upper water layers, CoLM-Snicar can strengthen mid-depth cold biases when turbulent mixing, entrainment, seasonal overturning, or unresolved three-dimensional circulation fails to transport sufficient heat below the thermocline. This interpretation is consistent with previous evaluations of 1-D lake models, which show that vertical temperature profiles are sensitive not only to light extinction but also to vertical mixing parameters and surface-exchange formulations (M. Guo et al., 2021; A. Huang et al., 2019; Q. Zhang et al., 2019). To diagnose the interaction between radiative transfer and vertical mixing, we perform an additional sensitivity experiment for Lake Nam Co, where the empirical vertical mixing coefficient is amplified by a factor of 100 while both CoLM-Default and CoLM-Snicar keep the same empirical water extinction formulation (Wu et al., 2020). The results show that the enhanced-mixing run significantly reduces the mid-depth cold bias in CoLM-Default by promoting downward heat transport, indicating that insufficient vertical mixing is a primary source of the heat-storage bias in Lake Nam Co (Fig. S11f). Once this first-order mixing error is alleviated, CoLM-Snicar produces additional improvements relative to the enhanced-mixing default run, showing that the spectral radiative-transfer scheme still adds skill when the host lake model represents vertical heat transport more realistically (Fig. S11g). These results suggest that CoLM-Snicar is most effective when radiative-transfer errors are a dominant contributor to the heat-budget bias. When biases are instead controlled by heat storage, mixing, or overturning, improved radiative transfer must be combined with improved parameterizations of vertical heat transport and ice processes.

Several uncertainties should be considered in future analyses. First, water optical properties remain incompletely represented. Although this study uses observed or literature-based visible-band extinction coefficients, these values are prescribed as fixed lake-specific parameters and therefore cannot accurately capture seasonal variations in chlorophyll, colored dissolved organic matter, suspended sediments, or turbidity. The spectral absorption and scattering properties used by SNICAR-ADv5 are consequently only partially constrained by observations. Future work should link water optical properties to biogeochemical and sediment variables, or assimilate remotely sensed water-clarity products where available. Second, snow and ice optical parameters introduce significant uncertainty. SNICAR-ADv5 requires information on ice density, air-bubble radius, impurity loading, and snow and ice grain properties, but these variables are rarely observed for lakes. The MODIS-based inversion used in this study provides a practical constraint for lakes with sufficient snow-free bare-ice observations, but it is limited by cloud contamination, mixed pixels, spatial resolution, and the difficulty of isolating pure ice surfaces (Whicker et al., 2024). For lakes such as Harp and Ngoring, this inversion cannot be robustly implemented, and the default ice parameters provided by SNICAR-ADv5 must be used. We conduct sensitivity experiments based on the three inverted ice parameters for Lake Ngoring, and the results suggest that simulations using the default parameters are broadly representative of the range of possible CoLM-Snicar responses within the sampled valid parameter space (Fig. S12). Quantitatively, however, the use of default parameters

https://doi.org/10.5194/egusphere-2026-4210
Preprint. Discussion started: 22 July 2026

may still bias simulated albedo, ice transmittance, and under-ice heating, because bubble-rich ice, refrozen slush, and impurity-contaminated ice can strongly alter scattering and absorption (Dadic et al., 2013; Flanner et al., 2021; M. Wang et al., 2022; Weyhenmeyer et al., 2022). More lake-specific observations of ice optical and microphysical properties are therefore needed. Finally, uncertainties also arise from the selected 1-D lake model and from the evaluation datasets. CoLM-Lake does not represent horizontal circulation, lateral heat transport, inflows and outflows, or basin-scale internal waves, although these processes can be tightly coupled with radiative transfer and can strongly influence lake thermal structure in large, deep, or morphologically complex lakes. Under ice, seiche-driven turbulence can enhance basal heat flux and invalidate a purely conductive representation of the ice-water boundary layer (Kirillin et al., 2018), but this is also not included in CoLM-Lake. In addition, lake depth, meteorological forcing, extinction coefficients, ice thickness, and validation temperature profiles differ in accuracy among sites, and the nine-lake sample cannot fully represent global lake diversity. Therefore, the current evaluation demonstrates the process-level value of coupling SNICAR-ADv5 with CoLM-Lake, and broader applications should be further assessed using lake models with more detailed representations of mixing, circulation, and heat transport, together with lake observational datasets that more accurately characterize optical, thermal, and ice conditions.

6 Conclusions and future directions

In this study, we couple the 1-D lake model CoLM-Lake with the spectral radiative-transfer scheme SNICAR-ADv5 and treat the snow–ice–water column as a unified, optically active system to improve the representation of shortwave radiation transfer for lake columns. Compared with the original CoLM-Lake scheme, which primarily relies on opaque snow/ice assumptions and Beer-Lambert attenuation in water, the coupled CoLM-Snicar framework explicitly represents wavelength-dependent absorption and scattering, the separate propagation of direct and diffuse radiation, Fresnel reflection and transmission at interfaces between media, and multiple radiative interactions among snow, ice, and water layers. The model is evaluated across nine lakes spanning broad differences in depth, water clarity, climatic forcing, and ice-cover conditions.

The multi-lake evaluation demonstrates that the influence of CoLM-Snicar is physically consistent but lake dependent. During open-water periods, the most robust process-level effect of SNICAR-ADv5 is to redistribute absorbed shortwave energy toward the near-surface water layers, especially for diffuse radiation, while reducing radiative heating below the mixed layer. This redistribution improves simulated thermal structures in lakes where the original CoLM-Lake configuration produces overly deep thermoclines and excessive subsurface warming. The results also show that prescribing observation-based water extinction coefficients alone can substantially improve simulations in highly turbid lakes where the default empirical extinction values underestimate light attenuation. However, CoLM-Extinct remains structurally constrained by its single-band Beer-Lambert formulation. By contrast, CoLM-Snicar provides a more physically consistent radiative-heating profile, allowing model biases to be interpreted in terms of illumination geometry, spectral absorption, scattering, and interfacial transmission. Therefore, the coupled framework is not merely a parameter adjustment, but a process-based upgrade that improves the diagnostic capability of CoLM-Lake.

For seasonally ice-covered lakes, CoLM-Snicar enables shortwave energy to be partitioned among snow, ice, and underlying water rather than forcing all non-reflected radiation to be absorbed in the uppermost snow or ice layer. This treatment allows the model to represent internal ice heating, under-ice water warming, and basal melt pathways that are absent from the opaque-snow and opaque-ice approximation. The simulated impacts on ice phenology vary among lakes because they depend on snow cover, ice optical properties, water clarity, and under-ice heat storage. In several lakes, CoLM-Snicar delays ice break-up by reducing total shortwave absorption within the ice layer, whereas in Lake Ngoring it advances break-up by enhancing under-ice radiative warming and basal melt. These contrasting responses highlight the importance of resolving radiative transfer within the full snow-ice-water column when simulating lake-ice evolution.

Despite these improvements, the coupled model does not uniformly reduce errors across all lakes. In Lake Trout and Nam Co, where observations indicate substantial downward heat propagation and relatively deep thermoclines, the SNICAR-induced upward redistribution of absorbed shortwave radiation can partly intensify mid-depth cold biases, indicating the influence of other model uncertainties related to turbulent mixing, entrainment, convective adjustment, seasonal overturning, and deep heat storage. Therefore, the coupled model helps reveal whether dominant thermal biases arise from radiative transfer, vertical mixing, or their interaction. Its greatest benefit is expected in lakes where errors in the vertical distribution of shortwave heating are the primary source of thermal-structure bias.

Future applications of the coupled CoLM-Lake and SNICAR-ADv5 framework should move from process-level evaluation toward more transferable and prognostic lake simulations. Key priorities include representing seasonally evolving water clarity and snow-ice optical conditions, strengthening observational constraints from in situ measurements and satellite retrievals, and integrating the improved radiative-transfer treatment with more complete descriptions of mixing, overturning, and ice-water heat exchange. These developments are particularly important for deep, clear, or morphologically complex lakes, where radiative heating interacts strongly with vertical heat storage and transport. Overall, the coupled model provides a physically based and diagnostically useful framework for improving simulations of lake thermal structure, ice phenology, and lake-atmosphere interactions in land, weather, and Earth system models.

Code and data availability

The CoLM-Lake coupled with SNICAR-ADv5 source code (under the MIT license) with the simulation dataset used in this paper is provided on Zenodo at https://doi.org/10.5281/ZENODO.21396031 (Cao et al., 2026).

Author contributions

XC and NW conceived and designed the study, developed the model implementation, performed the simulations, analysed the data, prepared the figures and tables, and wrote the original manuscript. HY, SZ, ZW, XL, and LL reviewed and revised the manuscript. YD reviewed and revised the manuscript and provided project support, supervision and funding acquisition.

Financial support

This work is supported by the Guangdong Major Project of Basic and Applied Basic Research (grant no. 2021B0301030007), the National Key R&D Program of China (grant no. 2023YFB3002400), and the National Natural Science Foundation of China (under grant No. 42375166, 42475172, and 42375164). It is also supported by the Southern Marine Science and Engineering Guangdong Laboratory (Zhuhai) (No. SML2023SP216) and the specific research fund of The Innovation Platform for Academicians of Hainan Province (grant no. YSPTZX202143).

Acknowledgements

We thank Juan P. Tolento from the Department of Earth System Science, University of California, for helpful guidance on the use of SNICAR-ADv5. We thank the North Temperate Lakes LTER program for providing in situ observations from Lake Crystal Bog, Lake Trout, Lake Trout Bog, and Lake Sparkling; Frank Beyrich from the Lindenberg Meteorological Observatory, Germany, for providing data from Lake Kossenblatter; Huaxia Yao from the Environmental Monitoring and Reporting Branch, Ministry of Environment, Conservation and Parks, for providing data from Lake Harp; Xuhui Lee from Yale University for providing data from Lake Tai; Liping Zhu and his research team from the Institute of Tibetan Plateau Research, Chinese Academy of Sciences, for providing data from Lake Nam Co; Zhaoguo Li from the Northwest Institute of Eco-Environment and Resources, Chinese Academy of Sciences, for providing meteorological forcing data for Lake Ngoring; and Georgiy B. Kirillin from the Leibniz-Institute of Freshwater Ecology and Inland Fisheries, Berlin, Germany, for providing water temperature observations for Lake Ngoring. We also thank the Inter-Sectoral Impact Model Intercomparison Project 2a (ISIMIP2a) for providing extinction coefficient data for some of the lakes used in this study, and NASA for providing the MODIS remote sensing products used in this work. We also acknowledge the high-performance computing support from the School of Atmospheric Science at Sun Yat-sen University. The authors used a large language model, ChatGPT-5.5, to improve the language and readability of the manuscript. The authors thoroughly reviewed and edited the text as needed and take full responsibility for the final content of the publication.

Competing interests

The contact author has declared that none of the authors has any competing interests.

References

Bernus, A. and Ottlé, C.: Modeling subgrid lake energy balance in ORCHIDEE terrestrial scheme using the FLake lake model, Geosci. Model Dev., 15, 4275–4295, https://doi.org/10.5194/gmd-15-4275-2022, 2022.

Beyrich, F., Leps, J.-P., Mauder, M., Bange, J., Foken, T., Huneke, S., Lohse, H., Lüdi, A., Meijninger, W. M. L., Mironov, D., Weisensee, U., and Zittel, P.: Area-averaged surface fluxes over the litfass region based on eddy-covariance measurements, Bound.-Layer Meteorol., 121, 33–65, https://doi.org/10.1007/s10546-006-9052-x, 2006.

Briegleb, B. P.: Delta-Eddington approximation for solar radiation in the NCAR community climate model, J. Geophys. Res. Atmospheres, 97, 7603–7612, https://doi.org/10.1029/92JD00291, 1992.

Briegleb, B. P. and Light, B.: A Delta-Eddington multiple scattering parameterization for solar radiation in the sea ice component of the Community Climate System Model., National Center for Atmospheric Research, 2007.

Brun, E.: Investigation on wet-snow metamorphism in respect of liquid-water content, Ann. Glaciol., 13, 22–26, https://doi.org/10.3189/S0260305500007576, 1989.

Cao, X., Wei, N., Yuan, H., Zhang, S., Wei, Z., Lu, X., Li, L., and Yongjiu, D.: Code and Data for Improving Shortwave Radiative Transfer in the Lake Component of the Common Land Model (CoLM-Lake) with a Spectral Scheme for the Full Snow-Ice-Water Column, https://doi.org/10.5281/ZENODO.21396031, 2026.

Chang, X., Xue, M., Li, P., Wang, Q., and Zuo, G.: Experimental research on ice density measurement method based on ultrasonic waves, Water, 15, 4065, https://doi.org/10.3390/w15234065, 2023.

Chevrollier, L.-A., Cook, J. M., Halbach, L., Jakobsen, H., Benning, L. G., Anesio, A. M., and Tranter, M.: Light absorption and albedo reduction by pigmented microalgae on snow and ice, J. Glaciol., 69, 333–341, https://doi.org/10.1017/jog.2022.64, 2023.

Cole, T. M. and Wells, S. A.: CE-QUAL-W2: A Two-dimensional, Laterally Averaged, Hydrodynamic and Water Quality Model, Version 3.5, US Army Engineering and Research Development Center, Vicksburg, MS, 2006.

Cuffey, K. M. and Paterson, W. S. B.: The physics of glaciers, Fourth edition., Elsevier, San Diego, 1 pp., 2010.

Dadic, R., Mullen, P. C., Schneebeli, M., Brandt, R. E., and Warren, S. G.: Effects of bubbles, cracks, and volcanic tephra on the spectral albedo of bare ice near the Transantarctic Mountains: implications for sea glaciers on Snowball Earth, J. Geophys. Res. Earth Surf., 118, 1658–1676, https://doi.org/10.1002/jgrf.20098, 2013.

Dai, Y., Dickinson, R. E., and Wang, Y.-P.: A two-big-leaf model for canopy temperature, photosynthesis, and stomatal conductance, J. Clim., 17, 2281–2299, https://doi.org/10.1175/1520-0442(2004)017%3C2281:ATMFCT%3E2.0.CO;2, 2004.

Dai, Y., Wei, N., Huang, A., Zhu, S., Shangguan, W., Yuan, H., Zhang, S., and Liu, S.: The lake scheme of the Common Land Model and its performance evaluation, Chin. Sci. Bull., 63, 3002–3021, https://doi.org/10.1360/N972018-00609, 2018.

Danabasoglu, G., Lamarque, J.-F., Bacmeister, J., Bailey, D. A., DuVivier, A. K., Edwards, J., Emmons, L. K., Fasullo, J., Garcia, R., Gettelman, A., Hannay, C., Holland, M. M., Large, W. G., Lauritzen, P. H., Lawrence, D. M., Lenaerts, J. T. M., Lindsay, K., Lipscomb, W. H., Mills, M. J., Neale, R., Oleson, K. W., Otto-Bliesner, B., Phillips, A. S., Sacks, W., Tilmes, S., van Kampenhout, L., Vertenstein, M., Bertini, A., Dennis, J., Deser, C., Fischer, C., Fox-Kemper, B., Kay, J. E., Kinnison, D., Kushner, P. J., Larson, V. E., Long, M. C., Mickelson, S., Moore, J. K., Nienhouse, E., Polvani, L., Rasch, P. J., and Strand, W. G.: The Community Earth System Model version 2 (CESM2), J. Adv. Model. Earth Syst., 12, e2019MS001916, https://doi.org/10.1029/2019MS001916, 2020.

Dang, C., Fu, Q., and Warren, S. G.: Effect of snow grain shape on snow albedo, J. Atmospheric Sci., 73, 3573–3583, https://doi.org/10.1175/JAS-D-15-0276.1, 2016.

Dang, C., Zender, C. S., and Flanner, M. G.: Intercomparison and improvement of two-stream shortwave radiative transfer schemes in Earth system models for a unified treatment of cryospheric surfaces, The Cryosphere, 13, 2325–2343, https://doi.org/10.5194/tc-13-2325-2019, 2019.

Desgué-Itier, O., Melo Vieira Soares, L., Anneville, O., Bouffard, D., Chanudet, V., Danis, P. A., Domaizon, I., Guillard, J., Mazure, T., Sharaf, N., Soulignac, F., Tran-Khac, V., Vinçon-Leite, B., and Jenny, J.-P.: Past and future climate change effects on the thermal regime and oxygen solubility of four peri-alpine lakes, Hydrol. Earth Syst. Sci., 27, 837–859, https://doi.org/10.5194/hess-27-837-2023, 2023.

Flanner, M. G. and Zender, C. S.: Linking snowpack microphysics and albedo evolution, J. Geophys. Res. Atmospheres, 111, 2005JD006834, https://doi.org/10.1029/2005JD006834, 2006.

Flanner, M. G., Arnheim, J. B., Cook, J. M., Dang, C., He, C., Huang, X., Singh, D., Skiles, S. M., Whicker, C. A., and Zender, C. S.: SNICAR-ADv3: a community tool for modeling spectral snow albedo, Geosci. Model Dev., 14, 7673–7704, https://doi.org/10.5194/gmd-14-7673-2021, 2021.

Gu, H., Jin, J., Wu, Y., Ek, M. B., and Subin, Z. M.: Calibration and validation of lake surface temperature simulations with the coupled WRF-lake model, Clim. Change, 129, 471–483, https://doi.org/10.1007/s10584-013-0978-y, 2015.

Guo, M., Zhuang, Q., Yao, H., Golub, M., Leung, L. R., Pierson, D., and Tan, Z.: Validation and sensitivity analysis of a 1-D lake model across global lakes, J. Geophys. Res. Atmospheres, 126, https://doi.org/10.1029/2020JD033417, 2021.

Guo, S., Dai, Y., Yuan, H., and Liang, H.: Enhanced MODIS-derived ice physical properties within the Common Land Model (CoLM) revealing bare-ice–snow albedo feedback over Greenland, The Cryosphere, 19, 3553–3570, https://doi.org/10.5194/tc-19-3553-2025, 2025.

Hall, D. K., Riggs, G. A., Salomonson, V. V., DiGirolamo, N. E., and Bayr, K. J.: MODIS snow-cover products, Remote Sens. Environ., 83, 181–194, https://doi.org/10.1016/S0034-4257(02)00095-0, 2002.

Hao, D., Bisht, G., Rittger, K., Bair, E., He, C., Huang, H., Dang, C., Stillinger, T., Gu, Y., Wang, H., Qian, Y., and Leung, L. R.: Improving snow albedo modeling in the E3SM land model (version 2.0) and assessing its impacts on snow and surface fluxes over the Tibetan Plateau, Geosci. Model Dev., 16, 75–94, https://doi.org/10.5194/gmd-16-75-2023, 2023.

He, C., Flanner, M., Lawrence, D. M., and Gu, Y.: New features and enhancements in Community Land Model (CLM5) snow albedo modeling: description, sensitivity, and evaluation, J. Adv. Model. Earth Syst., 16, e2023MS003861, https://doi.org/10.1029/2023MS003861, 2024.

He, J., Yang, K., Li, X., Tang, W., Shao, C., Jiang, Y., and Ding, B.: China meteorological forcing dataset v2.0 (1951-2024), https://doi.org/10.11888/Atmos.tpdc.302088, 2025.

Heiskanen, J. J., Mammarella, I., Ojala, A., Stepanenko, V., Erkkilä, K., Miettinen, H., Sandström, H., Eugster, W., Leppäranta, M., Järvinen, H., Vesala, T., and Nordbo, A.: Effects of water clarity on lake stratification and lake-atmosphere heat exchange, J. Geophys. Res. Atmospheres, 120, 7412–7428, https://doi.org/10.1002/2014JD022938, 2015.

https://doi.org/10.5194/egusphere-2026-4210
Preprint. Discussion started: 22 July 2026

Hostetler, S. W. and Bartlein, P. J.: Simulation of lake evaporation with application to modeling lake level variations of Harney-Malheur Lake, Oregon, Water Resour. Res., 26, 2603–2612, https://doi.org/10.1029/WR026i010p02603, 1990.

Huang, A., Lazhu, Wang, J., Dai, Y., Yang, K., Wei, N., Wen, L., Wu, Y., Zhu, X., Zhang, X., and Cai, S.: Evaluating and improving the performance of three 1-D Lake models in a large deep lake of the central Tibetan Plateau, J. Geophys. Res. Atmospheres, 124, 3143–3167, https://doi.org/10.1029/2018JD029610, 2019.

Huang, L., Wang, X., Sang, Y., Tang, S., Jin, L., Yang, H., Ottlé, C., Bernus, A., Wang, S., Wang, C., and Zhang, Y.: Optimizing lake surface water temperature simulations over large lakes in China with FLake model, Earth Space Sci., 8, https://doi.org/10.1029/2021EA001737, 2021.

Huang, W., Zhao, W., Zhang, C., Leppäranta, M., Li, Z., Li, R., and Lin, Z.: Sunlight penetration dominates the thermal regime and energetics of a shallow ice-covered lake in arid climate, The Cryosphere, 16, 1793–1806, https://doi.org/10.5194/tc-16-1793-2022, 2022.

Iacono, M. J., Delamere, J. S., Mlawer, E. J., Shephard, M. W., Clough, S. A., and Collins, W. D.: Radiative forcing by long-lived greenhouse gases: calculations with the AER radiative transfer models, J. Geophys. Res. Atmospheres, 113, 2008JD009944, https://doi.org/10.1029/2008JD009944, 2008.

Joseph, J. H., Wiscombe, W. J., and Weinman, J. A.: The Delta-Eddington approximation for radiative flux transfer, J. Atmospheric Sci., 33, 2452–2459, https://doi.org/10.1175/1520-0469(1976)033%3C2452:TDEAFR%3E2.0.CO;2, 1976.

Kirillin, G., Leppäranta, M., Terzhevik, A., Granin, N., Bernhardt, J., Engelhardt, C., Efremova, T., Golosov, S., Palshin, N., Sherstyankin, P., Zdorovennova, G., and Zdorovennov, R.: Physics of seasonally ice-covered lakes: a review, Aquat. Sci., 74, 659–682, https://doi.org/10.1007/s00027-012-0279-y, 2012.

Kirillin, G., Wen, L., and Shatwell, T.: Seasonal thermal regime and climatic trends in lakes of the Tibetan highlands, Hydrol. Earth Syst. Sci., 21, 1895–1909, https://doi.org/10.5194/hess-21-1895-2017, 2017.

Kirillin, G., Aslamov, I., Leppäranta, M., and Lindgren, E.: Turbulent mixing and heat fluxes under lake ice: the role of seiche oscillations, Hydrol. Earth Syst. Sci., 22, 6493–6504, https://doi.org/10.5194/hess-22-6493-2018, 2018.

Kirillin, G., Shatwell, T., and Wen, L.: Ice-covered lakes of Tibetan Plateau as solar heat collectors, Geophys. Res. Lett., 48, e2021GL093429, https://doi.org/10.1029/2021GL093429, 2021.

Lazhu, Yang, K., Wang, J., Lei, Y., Chen, Y., Zhu, L., Ding, B., and Qin, J.: Quantifying evaporation and its decadal change for Lake Nam Co, central Tibetan Plateau, J. Geophys. Res. Atmospheres, 121, 7578–7591, https://doi.org/10.1002/2015JD024523, 2016.

Lazhu, Yang, K., Hou, J., Wang, J., Lei, Y., Zhu, L., Chen, Y., Wang, M., and He, X.: A new finding on the prevalence of rapid water warming during lake ice melting on the Tibetan Plateau, Sci. Bull., 66, 2358–2361, https://doi.org/10.1016/j.scib.2021.07.022, 2021.

Lee, X., Liu, S., Xiao, W., Wang, W., Gao, Z., Cao, C., Hu, C., Hu, Z., Shen, S., Wang, Y., Wen, X., Xiao, Q., Xu, J., Yang, J., and Zhang, M.: The Taihu eddy flux network: an observational program on energy, water, and greenhouse gas fluxes of a large freshwater lake, Bull. Am. Meteorol. Soc., 95, 1583–1594, https://doi.org/10.1175/BAMS-D-13-00136.1, 2014.

Li, X., Long, D., Huang, Q., and Zhao, F.: The state and fate of lake ice thickness in the Northern Hemisphere, Sci. Bull., 67, 537–546, https://doi.org/10.1016/j.scib.2021.10.015, 2022.

Li, Z., Lyu, S., Wen, L., Zhao, L., Ao, Y., and Meng, X.: Study of freeze-thaw cycle and key radiation transfer parameters in a Tibetan Plateau lake using LAKE2.0 model and field observations, J. Glaciol., 67, 91–106, https://doi.org/10.1017/jog.2020.87, 2021.

Lin, T.-S., He, C., Abolafia-Rosenzweig, R., Chen, F., Wang, W., Barlage, M., and Gochis, D.: Improved snow albedo evolution in Noah-MP land surface model coupled with a physical snowpack radiative transfer scheme, J. Hydrometeorol., 26, 185–200, https://doi.org/10.1175/JHM-D-24-0082.1, 2025.

Luijendijk, A.: Validation, calibration and evaluation of a Delft3D-FLOW model with ferry measurements, master's thesis, Delft University of Technology, 2001.

Ma, X., Yang, K., La, Z., Lu, H., Jiang, Y., Zhou, X., Yao, X., and Li, X.: Importance of parameterizing lake surface and internal thermal processes in WRF for simulating freeze onset of an alpine deep lake, J. Geophys. Res. Atmospheres, 127, e2022JD036759, https://doi.org/10.1029/2022JD036759, 2022.

Ma, X., Yang, K., Wang, B., Li, Z., Lazhu, Lu, H., Yao, X., and Chen, X.: Strong skin cooling and its impacts on lake thermal processes in a large lake on the Tibetan Plateau, J. Hydrometeorol., 25, 937–946, https://doi.org/10.1175/JHM-D-23-0192.1, 2024.

MacKay, M. D., Neale, P. J., Arp, C. D., De Senerpont Domis, L. N., Fang, X., Gal, G., Jöhnk, K. D., Kirillin, G., Lenters, J. D., Litchman, E., MacIntyre, S., Marsh, P., Melack, J., Mooij, W. M., Peeters, F., Quesada, A., Schladow, S. G., Schmid, M., Spence, C., and Stokesr, S. L.: Modeling lakes and reservoirs in the climate system, Limnol. Oceanogr., 54, 2315–2329, https://doi.org/10.4319/lo.2009.54.6_part_2.2315, 2009.

Magnuson, J. J., Carpenter, S. R., and Stanley, E. H.: North Temperate Lakes LTER: High Frequency Water Temperature Data - Crystal Bog Buoy 2005 - current, https://doi.org/10.6073/PASTA/800E42BF5421EB3D601A07245FF5750E, 2023a.

Magnuson, J. J., Carpenter, S. R., and Stanley, E. H.: North Temperate Lakes LTER: High Frequency Water Temperature Data - Trout Bog Buoy 2003 - current, https://doi.org/10.6073/PASTA/9535BBC321EBD512CD0E8B0F1D7821BE, 2023b.

Magnuson, J. J., Carpenter, S. R., and Stanley, E. H.: North Temperate Lakes LTER: Snow and Ice Depth 1982 - current, https://doi.org/10.6073/PASTA/038D117F5244B520F7F87EF41DBA7A31, 2023c.

Magnuson, J. J., Carpenter, S. R., and Stanley, E. H.: North Temperate Lakes LTER: High Frequency Water Temperature Data - Sparkling Lake Raft 1989 - current, https://doi.org/10.6073/PASTA/1C42EB74649CDFFC87DAF7F00B5083AD, 2026a.

Magnuson, J. J., Carpenter, S. R., and Stanley, E. H.: North Temperate Lakes LTER: High Frequency Water Temperature Data - Trout Lake Buoy 2004 - current, https://doi.org/10.6073/PASTA/AA7AC54C2D1E58FC5AABC2FE4CCCD573, 2026b.

Marcé, R., Pierson, D., Mercado-Bettin, D., Thiery, W., Tan, Z., and Schewe, J.: ISIMIP2a Simulation Data from the Global Lakes Sector (1.0), https://doi.org/10.48364/ISIMIP.530719, 2022.

Mironov, D., Heise, E., Kourzeneva, E., Ritter, B., Schneider, N., and Terzhevik, A.: Implementation of the lake parameterisation scheme FLake into the numerical weather prediction model COSMO, Boreal Environ. Res., 15, 13, 2010.

https://doi.org/10.5194/egusphere-2026-4210
Preprint. Discussion started: 22 July 2026

Notaro, M., Holman, K., Zarrin, A., Fluck, E., Vavrus, S., and Bennington, V.: Influence of the laurentian Great Lakes on regional climate, J. Clim., 26, 789–804, https://doi.org/10.1175/JCLI-D-12-00140.1, 2013.

Oveisy, A. and Boegman, L.: One-dimensional simulation of lake and ice dynamics during winter, J. Limnol., 73, 441–453, https://doi.org/10.4081/jlimnol.2014.903, 2014.

Picard, G., Libois, Q., Arnaud, L., Verin, G., and Dumont, M.: Development and calibration of an automatic spectral albedometer to estimate near-surface snow SSA time series, The Cryosphere, 10, 1297–1316, https://doi.org/10.5194/tc-10-1297-2016, 2016.

Riihelä, A., Bright, R. M., and Anttila, K.: Recent strengthening of snow and ice albedo feedback driven by Antarctic sea-ice loss, Nat. Geosci., 14, 832–836, https://doi.org/10.1038/s41561-021-00841-x, 2021.

Rooney, G. and Jones, I.: Coupling the 1-D lake model FLake to the community land-surface model JULES, Boreal Environ. Res., 15, 501–512, 2010.

Schneider, A., Flanner, M., De Roo, R., and Adolph, A.: Monitoring of snow surface near-infrared bidirectional reflectance factors with added light-absorbing particles, The Cryosphere, 13, 1753–1766, https://doi.org/10.5194/tc-13-1753-2019, 2019.

Scott, R. W. and Huff, F. A.: Impacts of the Great Lakes on regional climate conditions, J. Gt. Lakes Res., 22, 845–863, https://doi.org/10.1016/S0380-1330(96)71006-7, 1996.

Segelstein, D.: The complex refractive index of water [data set], https://mospace.umsystem.edu/xmlui/handle/10355/11599, 1981.

Shimada, R., Takeuchi, N., and Aoki, T.: Inter-annual and geographical variations in the extent of bare ice and dark ice on the Greenland Ice Sheet derived from MODIS satellite images, Front. Earth Sci., 4, https://doi.org/10.3389/feart.2016.00043, 2016.

Stamnes, K., Tsay, S.-C., Wiscombe, W., and Jayaweera, K.: Numerically stable algorithm for discrete-ordinate-method radiative transfer in multiple scattering and emitting layered media, Appl. Opt., 27, 2502, https://doi.org/10.1364/AO.27.002502, 1988.

Stepanenko, V., Martynov, A., Jöhnk, K. D., Subin, Z. M., Perroud, M., Fang, X., Beyrich, F., Mironov, D., and Goyette, S.: A one-dimensional model intercomparison study of thermal regime of a shallow, turbid midlatitude lake, Geosci. Model Dev., 6, 1337–1352, https://doi.org/10.5194/gmd-6-1337-2013, 2013.

Stepanenko, V., Jöhnk, K. D., Machulskaya, E., Perroud, M., Subin, Z., Nordbo, A., Mammarella, I., and Mironov, D.: Simulation of surface energy fluxes and stratification of a small boreal lake by a set of one-dimensional models, Tellus Dyn. Meteorol. Oceanogr., 66, 21389, https://doi.org/10.3402/tellusa.v66.21389, 2014.

Stepanenko, V., Mammarella, I., Ojala, A., Miettinen, H., Lykosov, V., and Vesala, T.: LAKE 2.0: a model for temperature, methane, carbon dioxide and oxygen dynamics in lakes, Geosci. Model Dev., 9, 1977–2006, https://doi.org/10.5194/gmd-9-1977-2016, 2016.

Su, D., Hu, X., Wen, L., Lyu, S., Gao, X., Zhao, L., Li, Z., Du, J., and Kirillin, G.: Numerical study on the response of the largest lake in China to climate change, Hydrol. Earth Syst. Sci., 23, 2093–2109, https://doi.org/10.5194/hess-23-2093-2019, 2019.

https://doi.org/10.5194/egusphere-2026-4210
Preprint. Discussion started: 22 July 2026

Subin, Z. M., Riley, W. J., and Mironov, D.: An improved lake model for climate simulations: Model structure, evaluation, and sensitivity analyses in CESM1, J. Adv. Model. Earth Syst., 4, M02001, https://doi.org/10.1029/2011MS000072, 2012.

Tan, Z., Zhuang, Q., and Walter Anthony, K.: Modeling methane emissions from arctic lakes: Model development and site-level study, J. Adv. Model. Earth Syst., 7, 459–483, https://doi.org/10.1002/2014MS000344, 2015.

Tan, Z., Yao, H., and Zhuang, Q.: A small temperate lake in the 21st century: dynamics of water temperature, ice phenology, dissolved oxygen, and chlorophyll a, Water Resour. Res., 54, 4681–4699, https://doi.org/10.1029/2017WR022334, 2018.

Tolento, J. P., Zender, C. S., and Whicker-Clarke, C. A.: Surface and atmospheric heating responses to spectrally resolved albedo of frozen and liquid water surfaces, J. Geophys. Res. Atmospheres, 129, e2023JD039824, https://doi.org/10.1029/2023JD039824, 2024.

Tong, Y., Feng, L., Wang, X., Pi, X., Xu, W., and Woolway, R. I.: Global lakes are warming slower than surface air temperature due to accelerated evaporation, Nat. Water, 1, 929–940, https://doi.org/10.1038/s44221-023-00148-8, 2023.

Toon, O. B., McKay, C. P., Ackerman, T. P., and Santhanam, K.: Rapid calculation of radiative heating rates and photodissociation rates in inhomogeneous multiple scattering atmospheres, J. Geophys. Res., 94, 16287–16301, https://doi.org/10.1029/JD094iD13p16287, 1989.

Verpoorter, C., Kutser, T., Seekell, D. A., and Tranvik, L. J.: A global inventory of lakes based on high-resolution satellite imagery, Geophys. Res. Lett., 41, 6396–6402, https://doi.org/10.1002/2014GL060641, 2014.

Wang, M., Wen, L., Li, Z., Leppäranta, M., Stepanenko, V., Zhao, Y., Niu, R., Yang, L., and Kirillin, G.: Mechanisms and effects of under-ice warming water in Ngoring Lake of Qinghai–Tibet Plateau, The Cryosphere, 16, 3635–3648, https://doi.org/10.5194/tc-16-3635-2022, 2022.

Wang, W., Lee, X., Xiao, W., Liu, S., Schultz, N., Wang, Y., Zhang, M., and Zhao, L.: Global lake evaporation accelerated by changes in surface energy allocation in a warmer climate, Nat. Geosci., 11, 410–414, https://doi.org/10.1038/s41561-018-0114-8, 2018.

Webster, K. E., Kratz, T. K., Bowser, C. J., Magnuson, J. J., and Rose, W. J.: The influence of landscape position on lake chemical responses to drought in northern Wisconsin, Limnology & Oceanography, 41, 977–984, https://doi.org/10.4319/lo.1996.41.5.0977, 1996.

Weyhenmeyer, G. A., Obertegger, U., Rudebeck, H., Jakobsson, E., Jansen, J., Zdorovennova, G., Bansal, S., Block, B. D., Carey, C. C., Doubek, J. P., Dugan, H., Erina, O., Fedorova, I., Fischer, J. M., Grinberga, L., Grossart, H.-P., Kangur, K., Knoll, L. B., Laas, A., Lepori, F., Meier, J., Palshin, N., Peternell, M., Pulkkanen, M., Rusak, J. A., Sharma, S., Wain, D., and Zdorovennov, R.: Towards critical white ice conditions in lakes under global warming, Nat. Commun., 13, 4974, https://doi.org/10.1038/s41467-022-32633-1, 2022.

Whicker, C. A., Flanner, M. G., Dang, C., Zender, C. S., Cook, J. M., and Gardner, A. S.: SNICAR-ADv4: a physically based radiative transfer model to represent the spectral albedo of glacier ice, The Cryosphere, 16, 1197–1220, https://doi.org/10.5194/tc-16-1197-2022, 2022.

https://doi.org/10.5194/egusphere-2026-4210
Preprint. Discussion started: 22 July 2026

Whicker, C. A., Antwerpen, R., Flanner, M. G., Schneider, A., Tedesco, M., and Zender, C. S.: The effect of physically based ice radiative processes on Greenland Ice Sheet albedo and surface mass balance in E3SM, J. Geophys. Res. Atmospheres, 129, e2023JD040241, https://doi.org/10.1029/2023JD040241, 2024.

Wu, Y., Huang, A., Lazhu, Yang, X., Qiu, B., Wen, L., Zhang, Z., Fu, Z., Zhu, X., Zhang, X., Cai, S., and Tang, Y.: Improvements of the coupled WRF-Lake model over Lake Nam Co, Central Tibetan Plateau, Clim Dyn, 55, 2703–2724, https://doi.org/10.1007/s00382-020-05402-3, 2020.

Wu, Y., Huang, A., Li, X., Wen, L., Lazhu, and Li, J.: Thermal response of large seasonally ice-covered lakes over Tibetan Plateau to climate change, J. Geophys. Res. Atmospheres, 129, e2023JD039935, https://doi.org/10.1029/2023JD039935, 2024.

Xiao, W., Zhang, Z., Wang, W., Zhang, M., Liu, Q., Hu, Y., Huang, W., Liu, S., and Lee, X.: Radiation controls the interannual variability of evaporation of a subtropical lake, J. Geophys. Res. Atmospheres, 125, e2019JD031264, https://doi.org/10.1029/2019JD031264, 2020.

Xu, L., Liu, H., Du, Q., and Wang, L.: Evaluation of the WRF-lake model over a highland freshwater lake in southwest China, J. Geophys. Res. Atmospheres, 121, https://doi.org/10.1002/2016JD025396, 2016.

Yao, H., Samal, N. R., Joehnk, K. D., Fang, X., Bruce, L. C., Pierson, D. C., Rusak, J. A., and James, A.: Comparing ice and temperature simulations by four dynamic lake models in Harp Lake: past performance and future predictions, Hydrol. Process., 28, 4587–4601, https://doi.org/10.1002/hyp.10180, 2014.

Yao, X., Yang, K., Letu, H., Zhou, X., Wang, Y., Ma, X., Lu, H., and La, Z.: Observation and process understanding of typical cloud holes above lakes over the Tibetan Plateau, J. Geophys. Res. Atmospheres, 128, e2023JD038617, https://doi.org/10.1029/2023JD038617, 2023.

Zhang, Q., Jin, J., Wang, X., Budy, P., Barrett, N., and Null, S. E.: Improving lake mixing process simulations in the Community Land Model by using K profile parameterization, Hydrol. Earth Syst. Sci., 23, 4969–4982, https://doi.org/10.5194/hess-23-4969-2019, 2019.

Zhang, R., Wang, H., Fu, Q., Rasch, P. J., and Wang, X.: Unraveling driving forces explaining significant reduction in satellite-inferred Arctic surface albedo since the 1980s, Proc. Natl. Acad. Sci., 116, 23947–23953, https://doi.org/10.1073/pnas.1915258116, 2019.

Zhang, Y., Qin, B., Shi, K., Zhang, Y., Deng, J., Wild, M., Li, L., Zhou, Y., Yao, X., Liu, M., Zhu, G., Zhang, L., Gu, B., and Brookes, J. D.: Radiation dimming and decreasing water clarity fuel underwater darkening in lakes, Sci. Bull., 65, 1675–1684, https://doi.org/10.1016/j.scib.2020.06.016, 2020.

Zhou, X., Lazhu, Yao, X., and Wang, B.: Understanding two key processes associated with alpine lake ice phenology using a coupled atmosphere-lake model, J. Hydrol. Reg. Stud., 46, 101334, https://doi.org/10.1016/j.ejrh.2023.101334, 2023.

Zolfaghari, K., Duguay, C. R., and Kheyrollah Pour, H.: Satellite-derived light extinction coefficient and its impact on thermal structure simulations in a 1-D lake model, Hydrol. Earth Syst. Sci., 21, 377–391, https://doi.org/10.5194/hess-21-377-2017, 2017.